Basin Research

WILEY

Basin Research IAS EAGE

RESEARCH ARTICLE OPEN ACCESS

Source-to-Sink Signal Propagation in a Small, Coupled Catchment-Deep-Sea Fan System: The Sithas Example From the Corinth Rift (Pleistocene, Greece)

N. Deiss[1,2] | S. Rohais[1] | V. Regard[2] | J. J. Armitage[1] | S. Carretier[2] | S. Bonnet[2]

[1]IFP Energies Nouvelles, Rueil-Malmaison Cedex, France | [2]GET, University of Toulouse (UPS/CNRS/IRD/CNES), Toulouse, France

Correspondence: N. Deiss (nolwenn.deiss@ifpen.fr)

Received: 15 July 2024 | **Revised:** 4 June 2025 | **Accepted:** 8 June 2025

Funding: This work was supported by IFP Energies Nouvelles.

Keywords: glacial cycles | mass balance | quaternary | sediment supply | sedimentary budget | temporary storage

ABSTRACT

Quantifying sediment fluxes is an essential part of the Source-to-Sink approach in the understanding of sedimentary systems. However, the transfer of sediment from the source to the sink and the factors controlling it are still poorly understood. We focus on a small catchment coupled with its offshore deep-sea fan: the Sithas system (Gulf of Corinth, Greece). We restore the volume of sediment eroded in the catchment using geomorphic constraints; quantify the volume of sediment deposited in the offshore basin, after revising the age model; and calculate erosional fluxes using the BQART model. This allows for the comparison of the reconstructed fluxes of sediment eroded and deposited since 800 ka across the entire source-to-sink system. For the Sithas coupled catchment-deep-sea fan system, we show an increase in sedimentary fluxes both in erosion and deposition since 800 ka and particularly since 400 ka, where cyclic variations of ~120 kyr are recorded in erosion and deposition compartments. We suggest that the overall increase in flux results from a change in the catchment size due to the tectonic evolution of the region. The record of cyclic variations from 400 kyr in fluxes matches with the maturity of the system and with the intensification of glacial cycles and tectonic constraints migration. We also suggest that the discrepancy between erosion and deposition reflects a temporary storage between source and sink areas, probably along the coast. This has changed since 30 ka, introducing the last phase of evolution characterised by phased source and sink dynamics, suggesting a lack of temporary storage and a connection between river outlet and submarine canyon head. This study shows that sediment fluxes are controlled by the catchment's size as well as by climatic and tectonic factors and that even a small sedimentary system can be affected by temporary sediment storage.

1 | Introduction

Signals of tectonic and climatic change can be recorded in the sedimentary record through erosional fluxes in the source and depositional fluxes in the sink. The external forcing parameters that drive sediment erosion, transport and deposition, referred to as controlling factors, undergo various transformations. These include attenuation, phase-shifts that introduce lag times and even shredding (see for example the reviews of Allen 2008; Romans et al. 2016; Tofelde et al. 2021; Castelltort et al. 2023). In the natural environment, source-to-sink (S2S) signal transfer has been explored in many different settings, with a particular emphasis on the stratigraphic record. For example, during significant climatic shifts like the Palaeocene-Eocene thermal maximum (PETM), lag times of the order of 100 kyr are observed between sediment deposition and climate change, as indicated by isotopes (Duller et al. 2019). However, for these ancient records, the catchments no longer exist; only the preserved sink of the source-to-sink system is studied (Allen 2008). Indirect methods, such as BQART (Syvitski and Milliman 2007;

Summary

- Gradual increase of fluxes both in erosion and deposition since 800 ka especially since 400 ka.
- Climate and tectonic controlling factors on the coupled system, as well as the system's size growth.
- Erosion and deposition not in phase, probably due to temporary storage between source and sink.
- Transition from out-of-phase to in-phase dynamics and river–submarine canyon connection.

Watkins et al. 2019), can be useful to reconstruct the behaviour of former catchments.

Following Ronov et al.'s work in Ronov et al. 1980, numerous studies have investigated the estimation of sediment budgets to discuss the internal and external dynamics of sedimentary basins (see Hinderer 2012 for an overview). New methods to account for uncertainties in sediment budget calculations have recently been developed (Rouby et al. 2009; Guillocheau et al. 2012; Rohais et al. 2021), or for quantifying sediment transfer duration using tracers, for example, cosmogenic nuclides (see Repasch et al. 2020) or luminescence signal (OSL, see Guyez et al. 2023). Despite this interest in the source-to-sink approach and the sediment supply signal, there is in fact very few studies of entire systems including quantification of both catchment (Source) and sedimentary basin (Sink) (Pazzaglia and Brandon 1996; Somme et al. 2011; Rohais and Moretti 2017; Baudin et al. 2020). Most studies focus only on the source part or the sink part of a system. Studies that focused on both parts of the system demonstrated that the interaction of source with sink can modulate the erosion dynamics and related sediment supply evolution (Allen 2008; Rohais et al. 2012). This highlights the importance of investigating S2S systems as a whole.

The response of the source-to-sink system to periodic changes in climate can be categorised into three effects: (1) amplitude changes, (2) phase shifts and (3) signal shredding.

1. Amplitude changes: Numerical models of the detachment and transport of sediment by flowing water within the river channel have suggested that high frequency changes in discharge can amplify the sediment flux signal to the sink (Simpson and Castelltort 2012). Further down system, within the alluvial plain, the diffusive nature of the transport equations has been used to suggest signals will be damped, with a reduction in amplitude (e.g., Castelltort and van den Driessche 2003; Armitage et al. 2011; Straub et al. 2020). It is also possible that the landscape resonates to the frequency of the input forcing signal (Straub et al. 2020), where depending on the scale of the catchment high frequency forcing amplifies the signal while low frequencies are damped (Godard et al. 2013).
2. Phase shifts: The record in the sink can lag the input forcing, as has been observed for the PETM (Jones et al. 2004; Duller et al. 2019). In numerical models of landscape erosion and sediment transport, a phase shift is recorded with cyclic forcing (Simpson and Castelltort 2012; Braun et al. 2015; Armitage et al. 2018). This lag time suggests that there is a delay between erosion within the upper reaches of the catchment and the arrival of the signal within the alluvial plain and eventual sedimentary sink. Application of a sediment transport that includes a more complete treatment of the relationship between water discharge and sediment transport has found that there can potentially be negative lag times within the sedimentary system, where the response to cyclic change is skewed such that the peak in sediment flux precedes the peak of the imposed signal when the water flow is varied (McNab et al. 2023).
3. Signal Shredding: Periodic signals may however be indistinguishable from autogenic signals caused by interactions between the components of the source-to-sink system. This has been termed signal shredding (Jerolmack and Paola 2010), which Griffin et al. (2023) redefine as 'the smearing of externally driven signals by sediment transport processes [...] resulting in the amplitude of the environmental signal being severely degraded when compared to the amplitude of the original signal'. Below a critical frequency, defined by the transition from red to blue noise, external signals will be degraded in amplitude and potentially indistinguishable from the internal noise or autogenics of the system (Griffin et al. 2023). Laboratory-scale fluvial sediment transport experiments have been used to suggest that this critical frequency at a catchment scale could be of the order of 10^5 kyr (Toby et al. 2019).

In summary, a complex picture emerges from the numerical and laboratory experiments of signal amplification, shift and loss (e.g., Simpson and Castelltort 2012). In nature, understanding and quantifying the sedimentary signal from the source to the sink is confounded by loss of the source region due to tectonics and landscape change. It is therefore important to explore source-to-sink signals in closed and preserved catchment to basin systems. If the allogenic signal is strong enough to resist being erased by autogenic processes, it may still weaken and change as it moves through different parts of the sediment transport system, some sediment temporarily stored in intermediate 'reservoirs' along the way. For this reason, the residence time of sediment needs to be explored in the system; particularly the various possibilities for the sediments to be temporarily stored in intermediate reservoirs (e.g., floodplains, deltas and lakes) (Carretier et al. 2019). It is important to note that the response time is not a singular characteristic, varying based on the system's size, active processes and the nature of the disturbance. For instance, Castelltort et al. (2023) consider that the response time of erosion related to long term uplift is longer than the response time related to precipitation and climatic variations, that means that uplift has an impact on landscapes over a longer time scale than climate. Similarly, the transfer system, such as rivers and their floodplains, generally responds more slowly to increased sediment supply than to increased water supply (Castelltort et al. 2023). Also, erosion may require an extended period to adapt to new conditions of faster or higher magnitude uplift and a shorter

period to adjust to slower or lower magnitude uplift conditions (Whipple 2001). Lastly, the geomorphic response to a climate change of a particular catchment will differ depending on the frequency and timescale of the change (Godard et al. 2013; Braun et al. 2015; Moussirou and Bonnet 2018).

We focus on the Sithas catchment and its deep-sea fan. The short source-to-sink distance should allow simple and direct signal propagation. This source-to-sink system is affected by Quaternary climatic variations characterised by variations in temperature, rainfall and eustatic level. At the regional scale, the climatic variations have been recorded with various phasings in the sediments (Collier 1990; McNeill et al. 2019; Watkins et al. 2019). The sediment flux can be estimated from the quantity of erosion in the source region and the rate of sediment deposition. These can be estimated in the sink region using offshore imagery of sediment thicknesses and in the source region using marine terraces that fossilise various stages in the development of this small catchment. Our objective is thus to jointly estimate erosion and sediment deposition across the entire source-to-sink system and subsequently discuss the influencing factors and the signal propagation mode. To achieve this, for both the source and the sink areas, we developed an age model (based, respectively, on marine terraces and seismic reflectors) and reconstructed the fluxes of sediment eroded in the catchment and deposited in the basin during the last 800 ka Quaternary climatic cycles with a resolution as good as 25 kyr for the last climatic cycle.

2 | Case Study: The Sithas System

The Sithas system, located near the city of Xylokastro on the southern coast of the Gulf of Corinth (Greece; Figure 1), comprises a 153.6 km^2-large catchment in the onshore domain, with a maximum elevation of 2376 m (Mount Ziria) coupled to a deep-sea fan offshore, with a maximal depth of −840 m (Figure 1B). The primary river in the catchment is the Sithas river, also known as the Trikalitikos river. The Gulf of Corinth, extensively studied for over 30 years, aligns with an active half-graben (Moretti et al. 2003) about 130 km long by 30 km wide, separating the

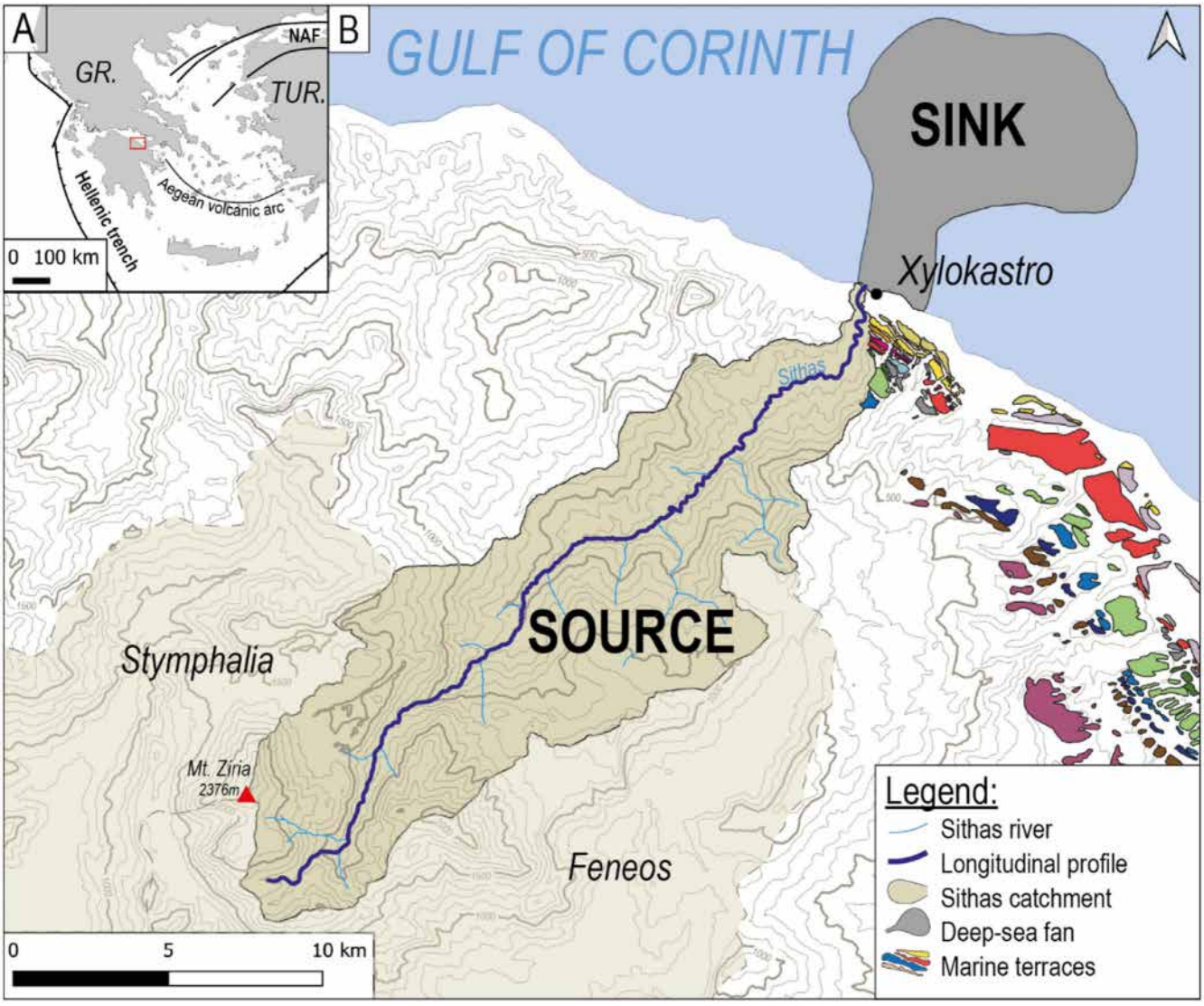

FIGURE 1 | (A) Simplified geodynamic setting of the Aegean region (modified from Demoulin et al. (2015) and Muravchik et al. (2020)) showing location of the Sithas area (red rectangle). GR, Greece; NAF, North Anatolian Fault; TUR, Turkey. (B) Map of the study area. Marine terraces from Armijo et al. (1996) and de Gelder et al. (2019), see Figure 3 for marine terraces' age.

Peloponnese from continental Greece since the Miocene. This zone stands out as the most tectonically active in Europe, with extension rates of approximately 1.5 cm yr^{-1} in a N-S direction to the west and 1.0 cm yr^{-1} to the east (Briole et al. 2000). The tectonic context generates an uplift rate during the last glacial–interglacial cycles of 1.3 mm yr^{-1} along the present-day coastline between Xylokastro and Corinth (Keraudren and Sorel 1987; Ori 1989; Armijo et al. 1996), increasing erosion and sedimentation processes (Schumm and Rea 1995; Rohais et al. 2021). This uplift, constant since 800 ka in this part of the Gulf, enables the preservation of marine terraces, with more than ten identified levels, making this area a world-class site for the study of marine terraces (Armijo et al. 1996; Pedoja et al. 2014; de Gelder et al. 2020). These marine terraces are part of the Upper Group (e.g., Rohais and Moretti 2017), a group characterised by stepped marine terraces and small deltas in the Xylokastro area since circa 800 ka, all lying above major unconformities cross-cutting the previous syn-rift units (Rohais and Moretti 2017). The long-term driver of tectonics enables us to study how the cyclicity overprints the tectonic in the Sithas system. For these different reasons, the Sithas system in the Gulf of Corinth stands as a unique case globally, allowing the restoration of palaeo-landscapes from stepped marine terraces and quantifying eroded volumes through an 'inverse' method. The Sithas system was also selected due to the extensive dataset available offshore with seismic lines calibrated with cores (Moretti et al. 2004) and wells (IODP, Shillington et al. 2019), giving us a well-constrained case study to investigate S2S.

3 | Data and Methods

3.1 | Markers and Age Model

3.1.1 | Onshore

The markers used for the onshore part correspond to marine terraces. Initially, we compiled all the terraces previously identified and mapped in the Xylokastro sector from previous studies (Armijo et al. 1996; de Gelder et al. 2019, 2020) and we checked the available absolute ages to date these terraces (Collier et al. 1992; Dia et al. 1997). For terraces lacking absolute age calibration, we used eustatic curves and the Marine Isotope Stage (MIS) ages from the work of Railsback et al. (2015) to assign ages (Figure 2), assuming that all terraces reflect a highstand condition related to the respective MIS peak.

In our study, we catalogued a total of 18 markers for the onshore part, including Kariotika 1 and 2, Melissi and Laliotis described by Armijo et al. (1996); Passio 1 and 2, New Corinth 1 and 2, Sataika 1 and 2, Old Corinth 1 and 2, Temple 1 and 2, Unnamed and Nicoletto from de Gelder et al. (2019); Holocene (de Gelder et al. 2020) and Topset Kryoneri (Rohais and Moretti 2017) (Figure 2).

3.1.2 | Offshore

The markers defined in the offshore part of the system, and their associated ages, came from three different studies: Nixon et al. (2016), McNeill et al. (2019) and Watkins et al. (2019). Nixon et al. (2016) used marine-lacustrine transitions with 100 kyr glacio-eustatic cycles. McNeill et al. (2019) used biozonations of calcareous nanofossils from well-cores combined with magneto-stratigraphic analyses to define marine dominated intervals and isolated basin intervals to then define an age model without specifying an uncertainty interval. Watkins et al. (2019) used marine-lacustrine transitions for their correlations between seismic horizons and piston-core data. We compiled all the dating to make a specific age model, with 13 markers: H1, H2 and H3 defined by Watkins et al. (2019), as well as H2 bottom (H4 equivalent of Watkins et al. (2019)), H3 top and bottom, H4 top and bottom, H5 top and bottom, H6 top and bottom and B-M from McNeill et al. (2019) and the absolute age markers determined by Gawthorpe et al. (2022) (Figure 2).

3.2 | Volume of Sediment Eroded From the Catchment

To recreate the volume of sediment eroded from the Sithas system for each time interval in the age model, we first reconstructed the shape of the palaeo-catchment associated with each of the marine terraces identified by Armijo et al. (1996) and de Gelder et al. (2019) with their corresponding age. These terraces were digitally represented in GIS software, on a 5 m resolution Digital Elevation Model (DEM) from the EU Copernicus program in 2016 (DEM provided by the National Cadastre & Mapping Agency S.A.). As the Sithas system is surrounded by marine terraces, we can follow the palaeo-coastline connecting the terraces on both side of the system at each time interval. For example, the 96 ka-old Melissi terrace lies 135 m above sea level, marking the present-day position of the ancient coastline. Except from the paleo-coastline point of Topset Kryonery (800 ka) determined by the actual outcrop of the delta, we continue the strike/orientation of the *inner edge* (i.e., southernmost mapped extent) of each terrace to where it intersects with the present day Sithas River catchment to define the most downstream part of the catchment. The interpreted palaeo-coastline can however be impacted by erosional morphologies generated afterwards that have impacted the mapped geometry on some of the terraces, especially the oldest terraces. There is therefore some uncertainty as to their location, for which we assume a margin of error of up to 100 m.

With the exception of schematic reconstruction D developed below, we assume that the upstream boundaries of the Sithas catchment remain fixed over time on the investigated time interval. This assumption is potentially valid as the catchment is located in the middle of the Mount Ziria massif and surrounded by two endorheic and fossil catchments: the Feneos and Stymphalia catchments (Zelilidis 2000; Rohais et al. 2007). The downstream part of each reconstructed palaeo-catchment is delimited by a palaeo-coastline point. The position of this point is shifted upstream for older palaeo-catchments in comparison with current catchment's outlet. The exact shape of the catchment for each time interval cannot be known. We therefore considered two scenarios about the shape of the catchment: in the first scenario we consider a minimum estimate; in the second senario we consider a maximum estimate (Figure 3). The first estimate aims to maintain the shape of the current catchment for each time interval, close

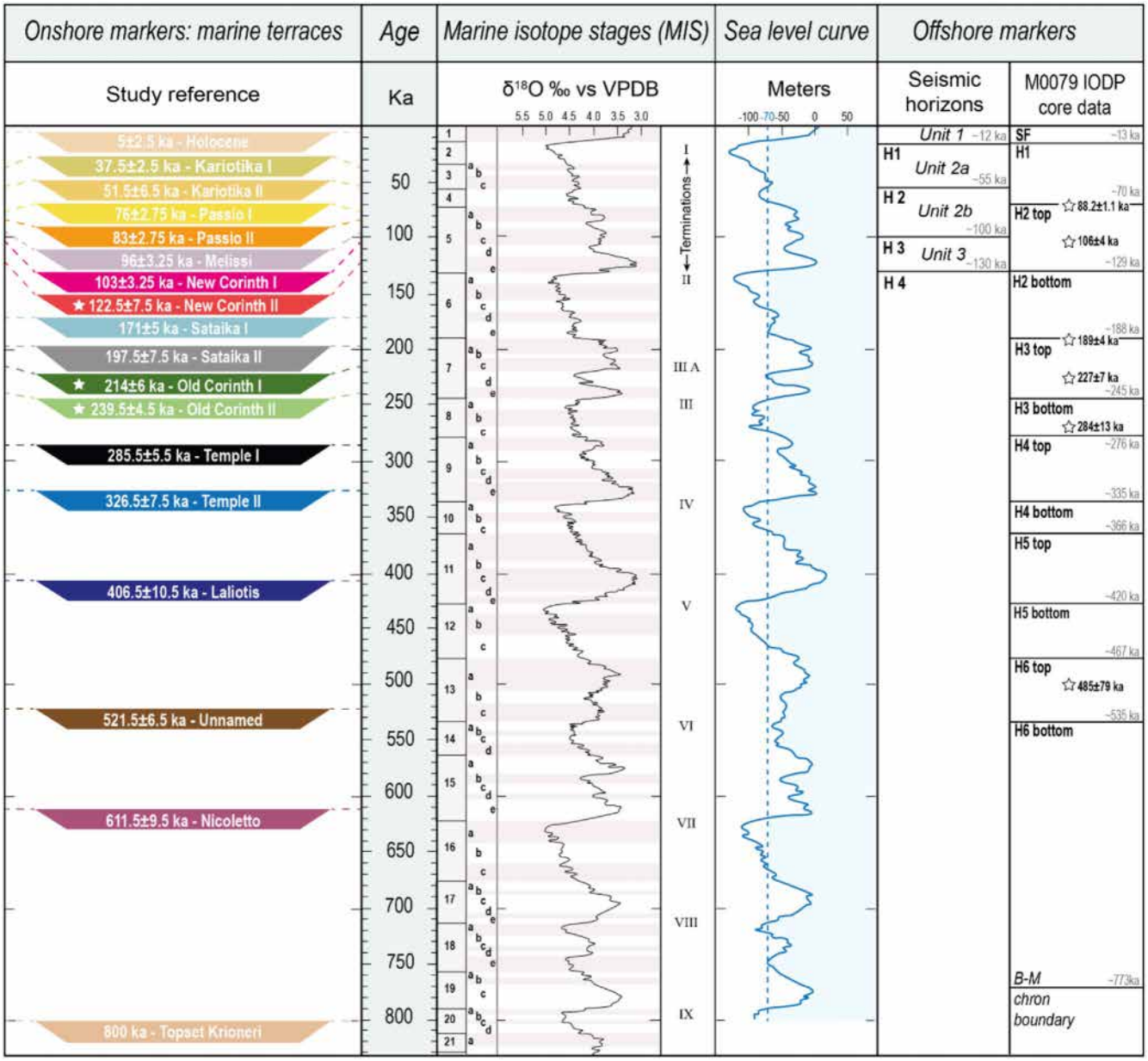

FIGURE 2 | Proposed age model of the Sithas system. Onshore markers and proposed ages modified from Armijo et al. (1996), de Gelder et al. (2019) and de Gelder et al. (2020), where ☆ figure dated terraces. Oxygen isotope curve and Marine Isotope Stages (MIS) from Railsback et al. (2015). Sea level curve from Spratt and Lisiecki (2016). Offshore markers from Nixon et al. (2016), Watkins et al. (2019) and McNeill et al. (2019). Absolute ages (☆) from Collier et al. (1992), Sébrier (1977), Leeder et al. (2005) and Gawthorpe et al. (2022).

to a homothetic shape (Figure 3A). For the second estimate of the palaeo-catchment shape, we followed the steepest line of the present-day topography from the palaeo-coastline point of each time interval to the present-day edge of the catchment. The upstream part of each palaeo-catchment corresponds to the present-day shape of the Sithas catchment (Figure 3B). The area of each palaeo-catchment version was then calculated (See Figure S1).

To evaluate the eroded volumes at each time interval (Figure 4A), we developed the four scenarios described below to calculate the catchment relief over time. These scenarios rely, without precise hillslope modelling, on the transverse profile of the valley and the longitudinal profile of the river in addition to the area of the catchment. First, we considered that the transverse profile is V-shaped, whose width is the current valley width. Second, we designed synthetic river profiles using four different assumptions (A to D, see below and Figure 4B). The eroded volume is the difference between the reconstituted catchment relief at two successive steps (Figure 4C).

The river profile reconstitution is first fixed to the current base level, and we replace each palaeo-coastline point along the river profile at the corresponding elevation of the associated and now uplifted marine terrace (e.g., the palaeo-coastline; points on Figure 4B). We then considered four schematic reconstructions to explore different concepts. It is important to note that although no single method is exact, the eroded volumes must lie between the four eroded volumes estimates.

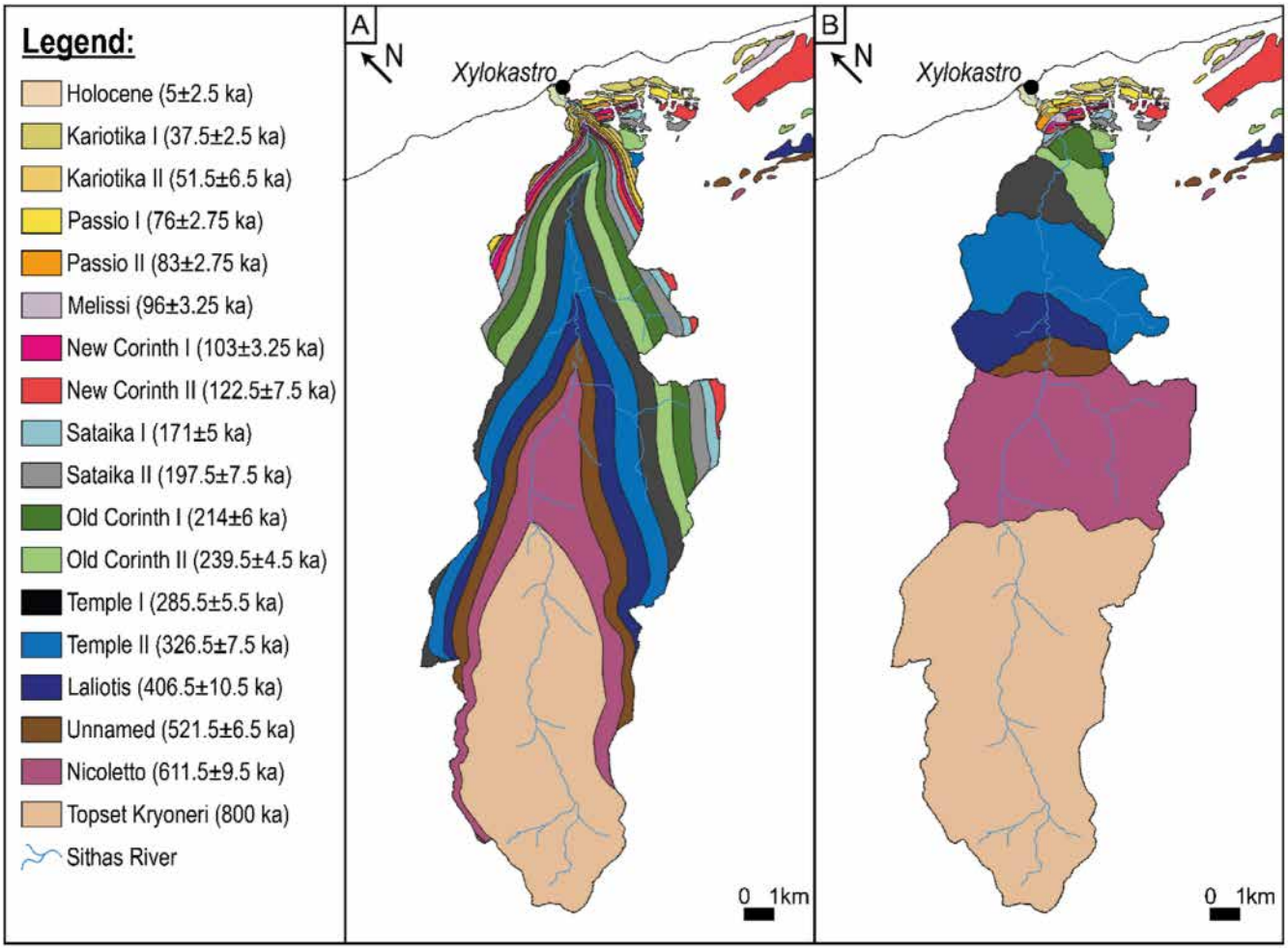

FIGURE 3 | Palaeo-catchment basin related to the marine terraces: Two end member reconstructions of its shape through time (see text for details). (A) 'Thin' palaeo-catchment. (B) 'Wide' palaeo-catchment.

- A: a scenario assuming cumulative vertical erosion along stream between two dated stages of the river profile evolution. We assume that river concavity is constant between these stages and does not change over time, as there is no direct correlation between river concavity and denudation rate leading to erosion (Whipple and Tucker 2002). The present river profile is vertically shifted so that it intersects the palaeo-coastline for each time interval. Of course, incision can occur in sudden bursts over the history of the river, resulting in knickpoints propagating upstream (de Lavaissière et al. 2022). These knick-points can be generated by sea-level variations during a glacial–interglacial cycle. Scenario A is not incompatible with the existence of knick-points. However, this scenario assumes that knick-points rise along the entire profile between two benchmark levels. This assumption is based on the observation that the only knick-point currently in existence on the Sithas River is at the head of the catchment (Zhou et al. 2024). However, it cannot be ruled out that one or more knick-points may have retreated more slowly. In this case, the estimated eroded volume would have to be restricted to the catchment area downstream of the knick-point. This situation is implicitly considered by Scenario D (see below).
- B: a purely geometric scenario with zero concavity in the downstream part. The ancient river profile is similar to the present day one from the source to the elevation of the corresponding palaeo-shoreline. The lower course of the river is then horizontal. Between two successive terraces, the crestline is vertical. This scenario is unrealistic; however, it gives a minimum estimate of the eroded volume.
- C: another geometric scenario called 'point-to-point'. Like B, except that the crestline is a simple line between the successive palaeo-shorelines.
- D: a capture scenario. Because several river capture occurrences have been recorded around the Gulf of Corinth (Watkins et al. 2019), we test the possibility of a capture of another now gone endorheic catchment. Today, relics of these captures can be found to the detriment of the Feneos and Stymphalia systems, which are now endorheic. A capture may have occurred at the same time as the Sataika II terrace development (around 200 ka), as there is a break in the slope of the river profile at this level. Such a capture should have driven first a vertical erosion in the downstream part by increasing the drainage area, and then a regressive erosion corresponding to the upstream propagation of an erosion wave. To model the corresponding river profile evolution, we shifted the present river profile first horizontally (0–600 ka) and then vertically,

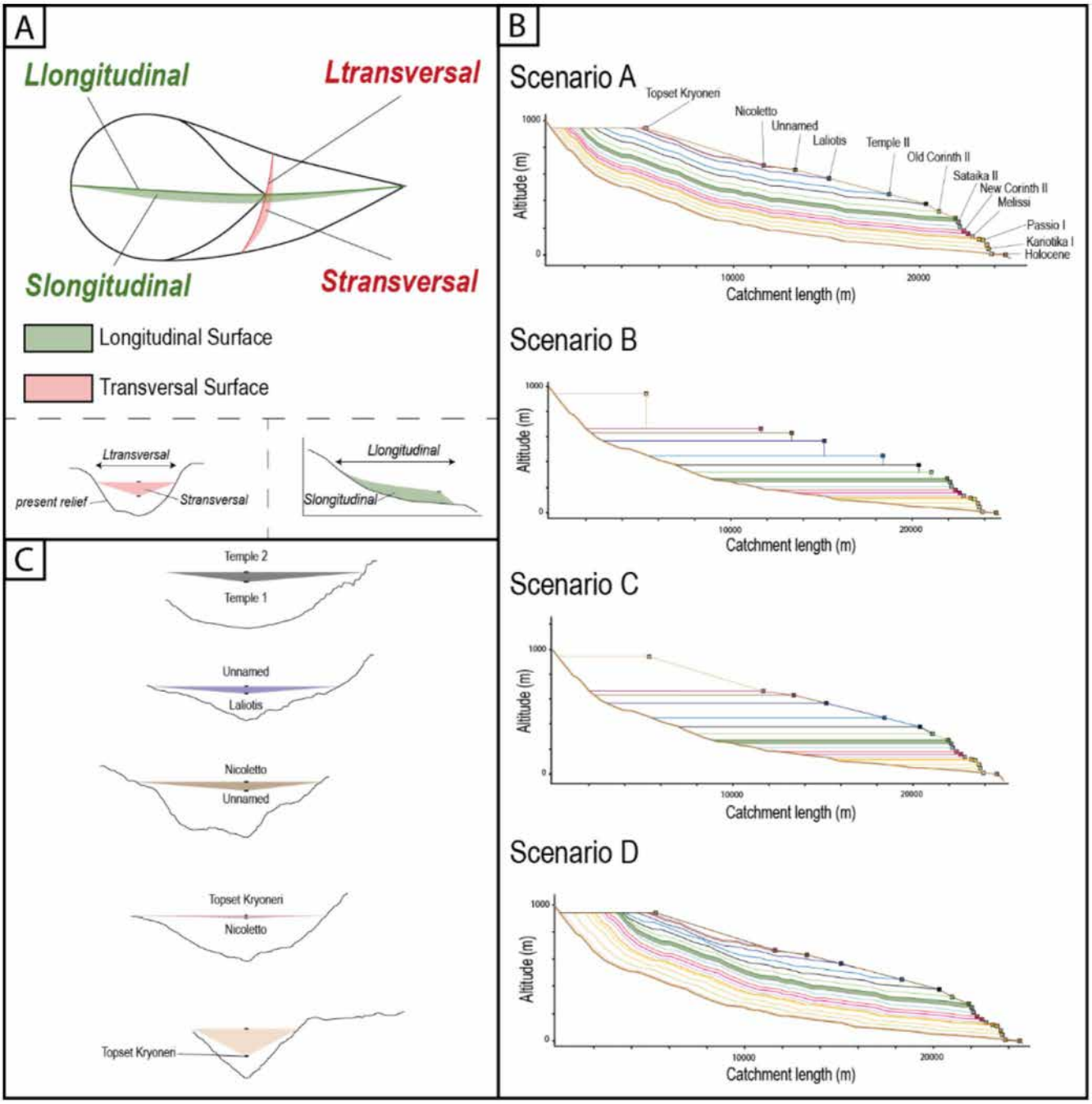

FIGURE 4 | (A) Schematic representation of the 'multi 2D' method; Llongitudinal = longitudinal length; Ltransversal = transversal length; Slongitudinal = longitudinal surface; Stransversal = transversal surface. (B) Transverse profiles (C) Longitudinal profiles of the Sithas system with the four scenarios (see description in part 3.2).

assuming constant river concavity as in scenario A. The offshore extent of the river profile is limited to the respective palaeo-coastline. As mentioned in senario A, this scenario is compatible with the gradual retreat of a knick-point, so that the erosion source area increases over time as the knick-point retreats.

Scenarios B and C are not realistic in terms of geomorphological evolution; nevertheless, they allow for the calculation of maximum and minimal eroded volumes.

The eroded volume of sediments is calculated as the average eroded thickness times the area for each time interval with the formula $V_{\text{eroded sed.}} = A \cdot E_{\text{moy}} \cdot 0.7$ where A is the palaeo-catchment area, E_{moy} is the average eroded thickness estimated as $E_{\text{moy}} = \frac{Slongitudinal + Stransversal}{Llongitudinal + Ltransversal}$ (Figure 4A) and 0.7 is the correction for a porosity factor of 30% as the catchment lithology is predominately limestones, conglomerates and sandstones (Rohais et al. 2007) (see Table S1 of Supporting Information). By normalising the eroded volumes with the maximum volume of 15.14 km^3 of rocks eroded, we aim to express the results in a

standardised way that accounts for variations in the sediment supply.

3.3 | Sediment Budget and Depositional Fluxes

A sediment budget was generated using 14 markers synthesised from literature data (Figure 2) correlated across the 2D seismic profiles from the R/V Maurice Ewing 2001 survey (Taylor et al. 2011) and the M.V. Vasilios 1996 survey (Figure 5). These horizons were the 12 horizons established from the IODP survey (McNeill et al. 2019) (H1 to Unit boundary, Figure 2), combined with 2 additional markers from Watkins et al. (2019) to increase resolution for the last 130 ka (Unit IIa and IIb in Watkins et al. (2019), Figure 2). Seismic stratigraphy was carried out to propagate manually the horizons over the study area in the Charisma software (GeoQuest), producing best estimate two-way travel time (TWTT) thickness maps. Interpolation was performed within the Charisma software to generate maps with a spatial resolution of 25 by 25 m. Depth converted maps were generated by applying a linear velocity model developed for the offshore Corinth rift by Nixon et al. (2016), as used in Watkins et al. (2019). This model uses a velocity increase of 1.5 $km^{-1}\,s^{-1}$ from the sea floor depth where the velocity is 1.55 $km^{-1}\,s^{-1}$ (see Nixon et al. (2016) for further details).

To establish the sediment budget of the Sithas deep-sea fan system, we delineated three possible fan extents (small, preferred and maximum) using the concepts of sequence stratigraphy on the seismic data and the interpretation of thickness maps for each time interval (Figures 5 and 6; Table S2 of Supporting Information) to explore a wide range of possibilities and take into account uncertainties in the mapping or the compaction of the sediments in deeper stratigraphy. These scenarios likely represent different deposition patterns within the Sithas sedimentary system as we cannot determine exactly the shape of the deep-sea fan during ancient times. We extracted deposited volumes related to the Sithas system by intersecting thickness maps with the contour masks of each submarine fan scenario using the QGIS software. The deposited volumes are converted into decompacted sediment volumes by applying a 46% porosity, which is estimated from the average values in the IODP wells (see Table S2 of Supporting Information) from the present-day thickness corrected with the linear velocity model detailed before. The sediment budget for the Sithas deep-sea fan finally results in 13 time intervals, with a minimal, maximal and preferred values.

3.4 | BQART Model

The BQART model, developed by Syvitski and Milliman (2007), is a global multi-regression empirical model designed to estimate suspended sediment load (Qs). It was established using a dataset from 488 global rivers. The expression for suspended sediment load in million tons per year (Mt/a) within catchments with average temperatures of ≥ 2°C is as follows:

$$Qs = \omega \cdot B \cdot Q^{0.31} \cdot A^{0.5} \cdot R \cdot T$$

where ω is a constant with a value of 0.0006 for units of Mt/a, B is a parameter that encompasses various effects such as lithology, Q is the catchment water discharge measured in cubic kilometres per year (km^3/a), A represents the drainage area of the catchment measured in square kilometres (km^2), R is the maximum relief in the catchment, measured in kilometres (km), T denotes the mean catchment-averaged annual temperature in degrees Celsius (°C) (Nyberg et al. 2021). If B is set to 1, Syvitski and Milliman (2007) demonstrate that the estimated sediment load accounts for 66% of the global variance in observed sediment load.

The BQART model has previously been applied to the entire Gulf of Corinth, covering the last 120 kyr (Watkins et al. 2019). In our study, we used the average temperature (T) and total precipitation (Q) of the four pollen assemblages determined by Mommersteeg et al. (1995) on the Tenagi Philippon cores located around 300 km to the North. The catchment area and its maximum relief were extracted from GIS data resulting from the restorations performed to estimate the volumes of eroded rock (refer to Section 3.2). As the predictions of the BQART are accurate to within a factor of 5, we focus on the relative change in flux over time rather than the flux magnitude at a given time.

Sediment supply, originally estimated in million tons per year (Mt/a), is reported in cubic kilometres per million years (km^3/Ma). To convert sediment loads from million tons per year to cubic metres per year of sediment, two densities were applied for a wider range of possibilities since the sediments in the study area originate from both silty conglomerates and sandstones: 1700 and 2250 kg/m^3.

3.5 | Comparison of Different BQART Model Parameters

In order to compare our results in detail, we compare the erosion versus suspended load (BQART) or deposition for different time periods. We defined the time periods by superimposing the periods defined for each of the signals. For each period thus defined, we extracted Mommersteeg et al. (1995)'s precipitation and temperature data, categorising them into three categories of precipitation (under 600 mm/yr, between 600 and 900 mm/yr and over 900 mm/yr) and two of averaged temperatures (under 13.5°C and over 13.5°C). We also determined the eustatic trends—lowstand, transgression, highstand and regression based on Spratt and Lisiecki (2016)'s sea level curve.

4 | Results

4.1 | Sediment Supply From Eroded Volumes

We estimated the sediment supply (km^3/Ma) from eroded volumes in the Sithas catchment basin over the last 800 ka in the form of erosion rates depending on the four scenarios adopted and presented in part 3.2 (Figure 6A–D). Erosional sediment fluxes are similar in magnitude for the 4 scenarios. The period between 800 and 400 ka is characterised by low fluxes, between 0.0 km^3/Ma (scenario D) and 10.9 km^3/Ma (scenario B), which increase progressively from 400 to 214 ka, with fluxes between

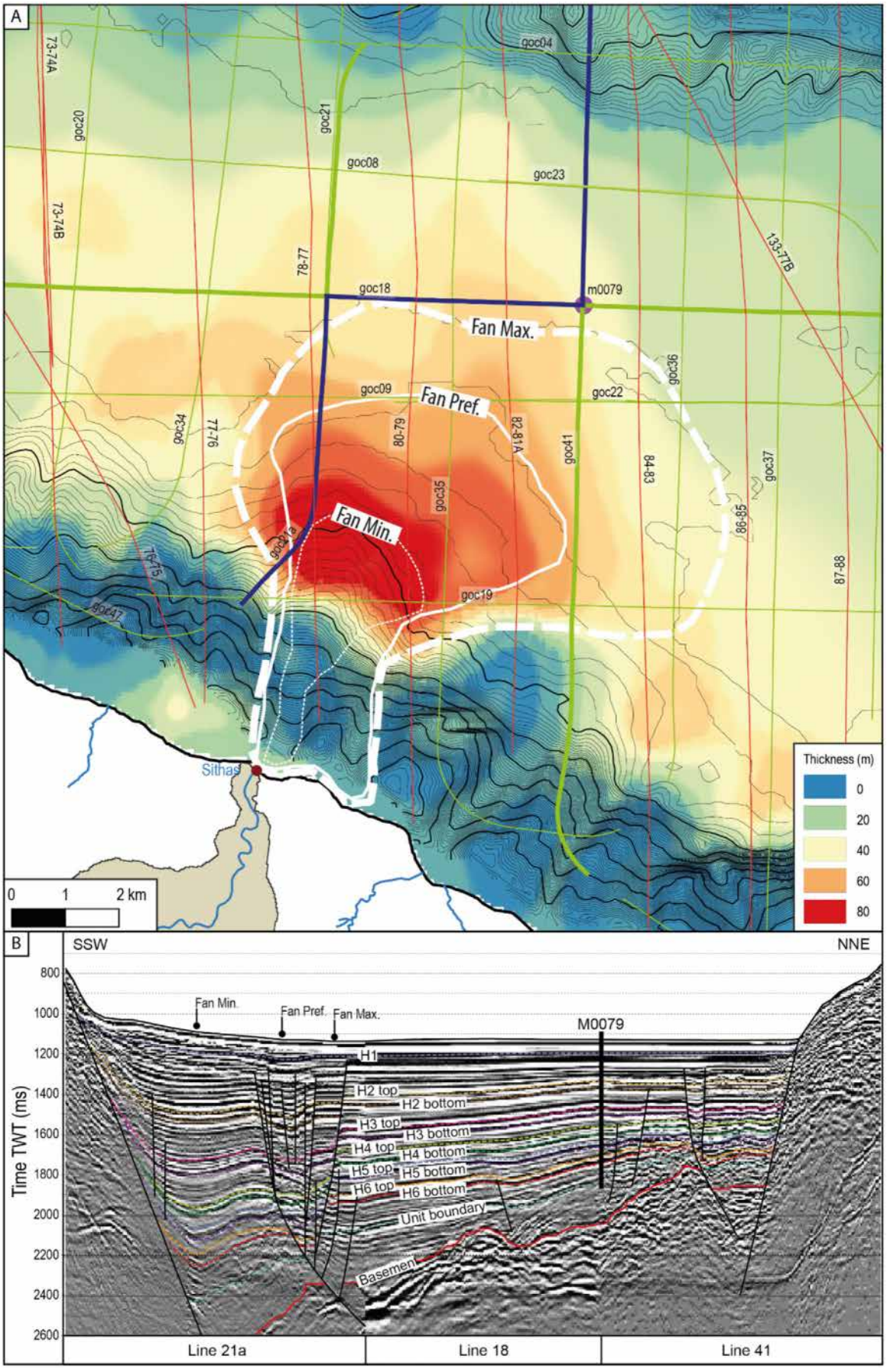

FIGURE 5 | Legend on next page.

FIGURE 5 | (A) Thickness Map of the studied case for the Holocene (H1 marker to Sea bottom = 12 ka); seismic lines from Taylor et al. (2011), Lykousis et al. (2007) and Sakellariou et al. (2007). (B) Chronostratigraphic framework using the markers by McNeill et al. (2019) on a composite high-resolution seismic reflection profile from Taylor et al. (2011), seismic lines used are highlighted in blue in (A).

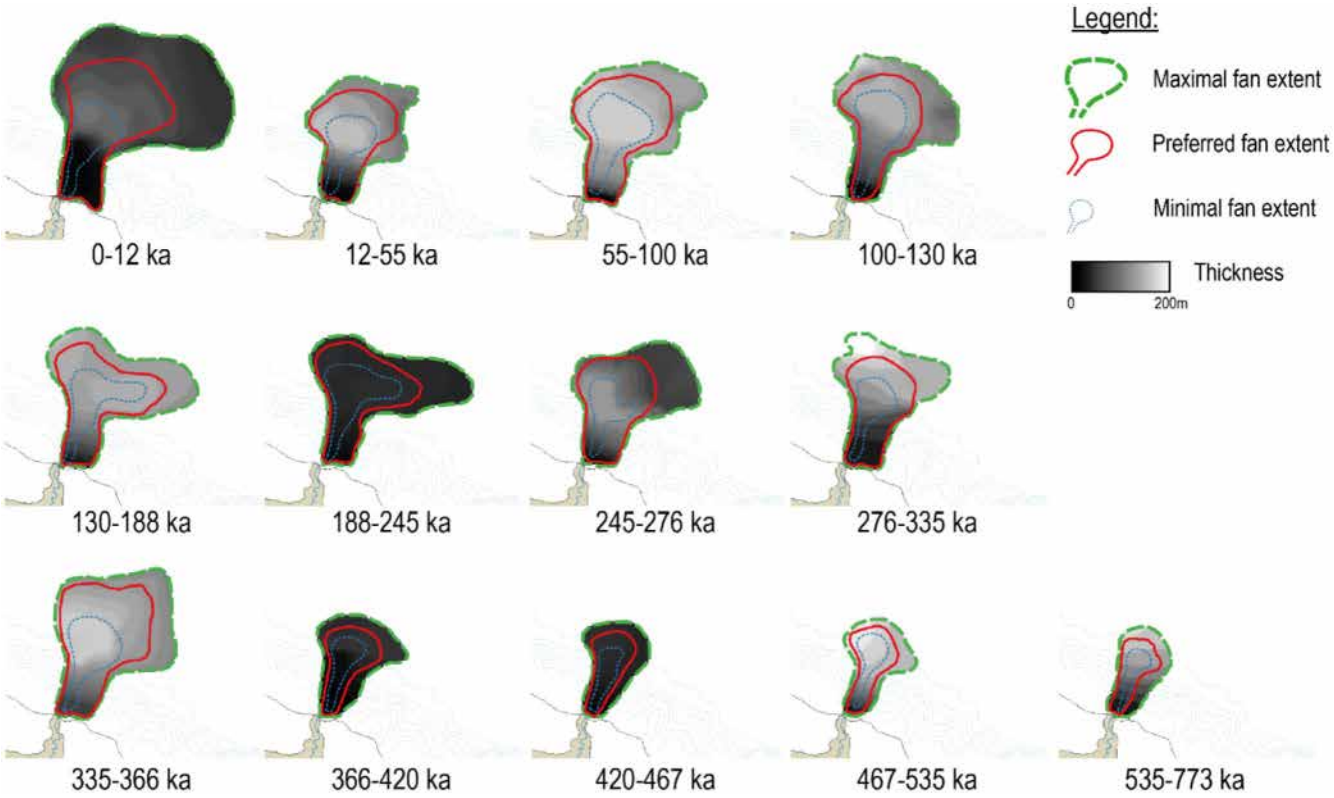

FIGURE 6 | Shape of the deep-sea fan for each time interval and each scenario, based on the thickness maps for each period of the age model.

7.1 km^3/Ma (scenario D) and 48.0 km^3/Ma (scenario A). There is then a decrease in flux between 220 and 150 ka, followed by many rapid variations (observed in part due to better model resolution) between 150 ka and the present day. A well-marked peak in fluxes occurred between 103 and 96 ka for all four scenarios (between 82.6 and 146.1 km^3/Ma). These trends, observed over the four scenarios, suggest that our results are robust. However, there are several differences between the fluxes in the different scenarios. Firstly, scenario D, representing the capture concept, has zero to very low fluxes for the 800–400 ka period. Fluxes between 400 and 120 ka are on the same order of magnitude as the three other scenarios, but still almost two times higher. Another difference is observed during the last 5 ka: a peak of fluxes is observed in both scenarios A and D; the flux for scenario D is two times the magnitude of scenario A, which is not the case for scenarios B and C, where sediment fluxes are approximately 4%–13% of those suggested by scenario A.

Among the four tested scenarios, the scenario A (with a mean catchment area) was the most geomorphologically consistent, so it is our preferred scenario. Fluxes of scenario A are initially low and consistent between 1.6 and 5.3 km^3/Ma from 800 to 400 ka. They then rise abruptly from 400 ka, with a maximum of 99.7 for the 103–96 ka period. Peaks in fluxes are observed at about 205, 100 and 5 ka and were as high as 50.0, 99.7 and 48.5 km^3/Ma, respectively. Between these peaks, fluxes seem to decrease gradually before increasing more rapidly, forming cycles of about 100 kyr. For the last 100 kyr-cycle, a peak of 72.6 km^3/Ma is registered at around 52 ka, thanks to a better resolution of our time intervals, suggesting a potential additional cyclicity of 50 ka.

4.2 | Sediment Supply From Deposited Volumes

The sediment supply from deposited volumes is considered according to three scenarios (minimal, preferred and maximal, see Figure 6) and the difference between maximal and minimal scenarios is depicted in grey in Figure 7E. Minimal and maximal scenarios exhibit significant value differences, especially during peak periods. Without considering the Holocene, maximal flux evaluations are 3.2 to 6.2 times higher than minimal evaluations. There is a progressive increase in sediment supply for 773 kyr, reaching 31.5 km^3/Ma (preferred scenario) from 100 to 55 ka. Several stages can be differentiated in a similar way we did for the sediment supply estimated from eroded volumes. An initial period (between 777 and 366 ka) is characterised by low and relatively stable flux of sediments deposited in the basin (1.0–6.8 km^3/Ma). The occurrence of four peaks, at approximately 366–335, 276–245, 100–55 and 12–0 kyr, indicates distinct cycles of growth and decline in sediment fluxes. The most recent peak also corresponds to the highest flux (75.0 km^3/Ma).

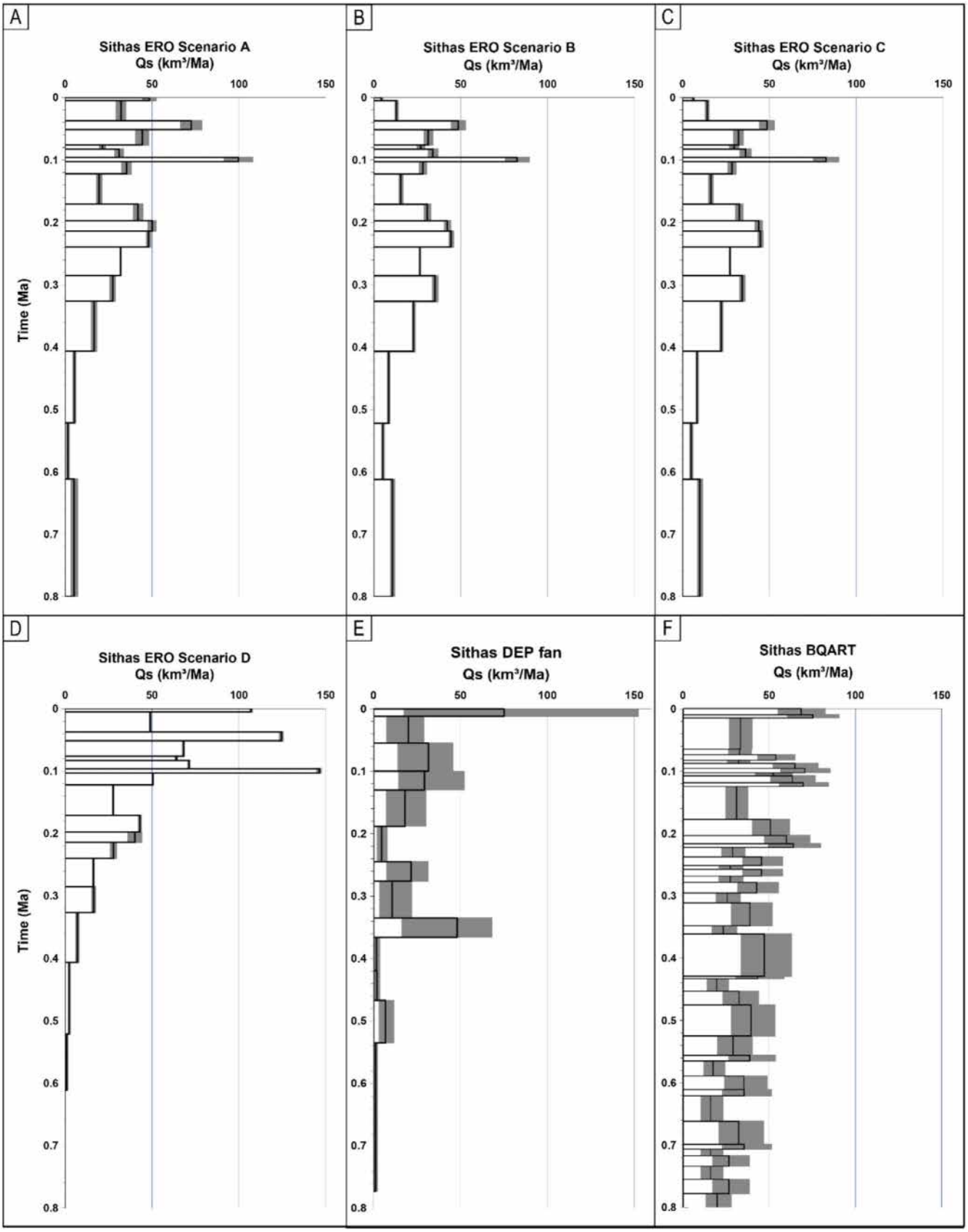

FIGURE 7 | (A–D) Sediment erosion flux (km^3/Ma) calculated over the last 800 ka depending on the four different scenarios described in part 3.2. (E) Sediment depositional flux (km^3 /Ma) over the last 800 ka, measured in the Sithas deep-sea fan. (F) Suspended sediment load (km^3 /Ma) over the last 800 ka calculated with the BQART method. (A–F) Solid lines represent mean flux and range of values are depicted in grey.

4.3 | BQART Fluxes

The sediment supply obtained using the BQART model (see Table S3 for the full data) follows an overall increasing trend, as do previous evaluations (Figure 6F). The average sediment fluxes predicted by BQART range from 16.2 to 76.7 km^3/Ma over the last 800 kyr. The time resolution of the BQART allows the observation of variations at high frequency (20 kyr). The results at this resolution cannot be compared with the other, less resolved, methods, so we focus on a 10^5 years-scale. At this scale, the temporal pattern is characterised by cycles occurring approximately every 100 kyr. The maximal fluxes during high-flux periods are up to 2.6 times greater than mean values for 800 kyr. The difference between successive high-flux and low-flux periods is approximately 1.5–1 for the period from 200 kyr.

4.4 | Comparison of Flux Evaluates

During the last 800 kyr, we estimated that 15.14 km^3 of sediments have been eroded and 9.04 km^3 (minimum of 3.49 km^3, maximum of 14.30 km^3) have been deposited for both preferred scenarios, which is ~60% the amount eroded. The estimations from the BQART model are around 32.30 km^3, that is, twice the volume of eroded sediment. The comparison of the three datasets (Figure 8) shows that the sediment fluxes computed with the BQART model are generally higher than those calculated from the erosional and depositional volumes. The comparison of the erosional and depositional sediment fluxes displays first a period of stability (800–400 ka) with low fluxes (between 3.0 and 7.2 km^3/Ma for erosion and 1.0 and 6.8 km^3/Ma for deposition) followed by a growth of the fluxes from 400 ka. Since then, the fluxes from the three methods show cyclic trends of around 100–120 ka with peaks at MIS 9 (325–285 ka), MIS 7 (225–190 ka) and MIS 5 (122–96 ka) for the erosional and BQART methods and peaks at MIS 10 (366–335 ka), MIS 8 (245–276 ka) and MIS 4 (100–55 ka) in deposition. There is an additional peak at MIS 3 (52–38 ka) happening in the erosional part of the system. All methods show a peak at MIS 1 (< 12 ka). The deposited peaks are therefore shifted in time in comparison with peaks observed in erosion, especially for the period between 310 and 130 ka. The trends are then registered both in erosion and deposition happened at the same time: low during MIS 2 and reaching a peak during MIS 1.

Figure 9 shows the ratio between depositional and erosional fluxes as a function of precipitation, temperature, eustatic level and erosion-BQART ratio (see Section 3.5 for methodology). When we compare the deposition-erosion ratio depending on the eustatic stage (Figure 9C), our results show that regression periods favour erosion but that transgression periods favour deposition and the stillstands seem to correspond to conditions close to steady state. In addition, high temperatures seem to generate strong fluxes, both in erosion and deposition. This graph, when modified to emphasise precipitation or temperature (Figure 9A,B), shows that erosional flux peaks occur when precipitation is high and the climate is warm (interglacial periods).

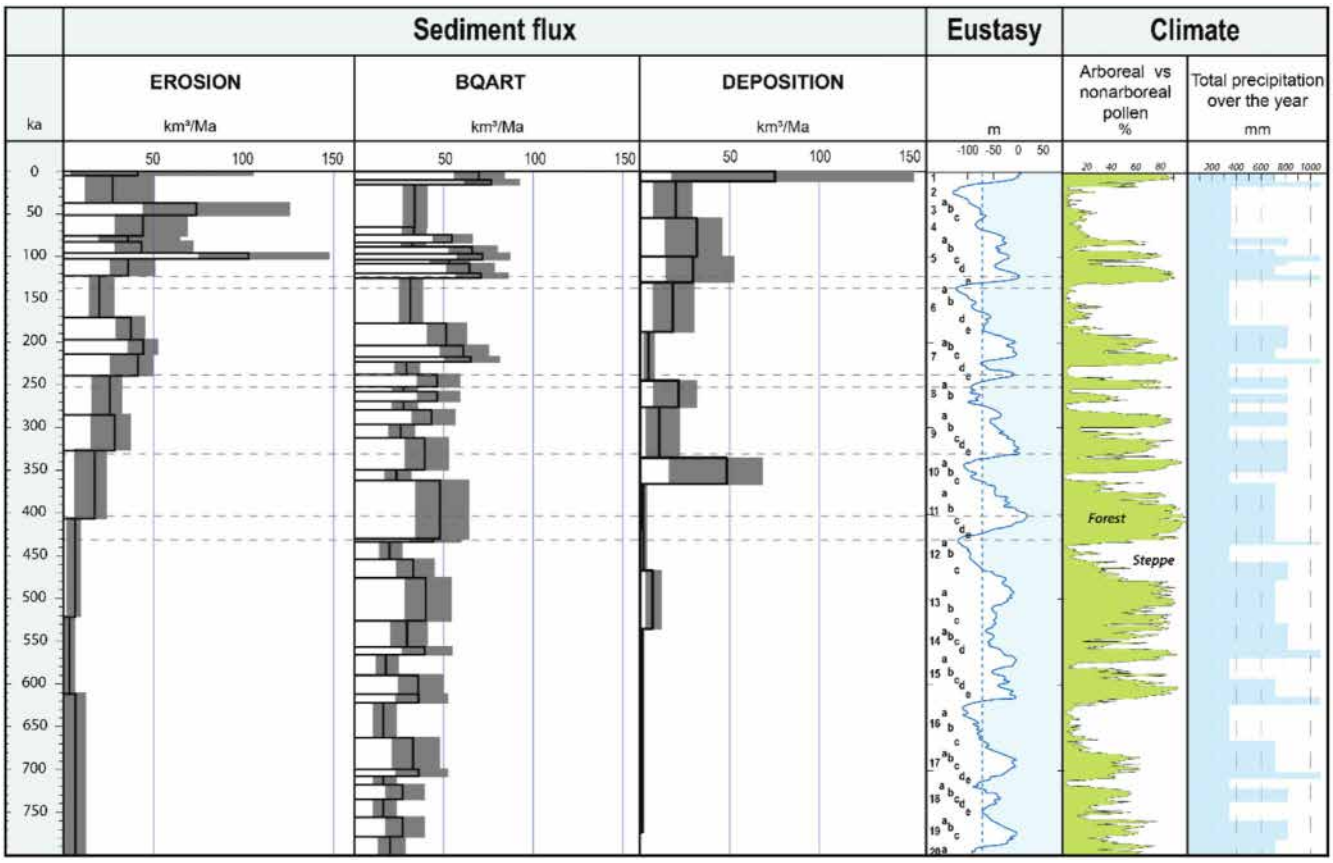

FIGURE 8 | Comparison of erosional scenario A, BQART and depositional fluxes (km^3/Ma) with eustasy and climate data. The horizontal dashed lines delimit the onset and end of each major transgression.

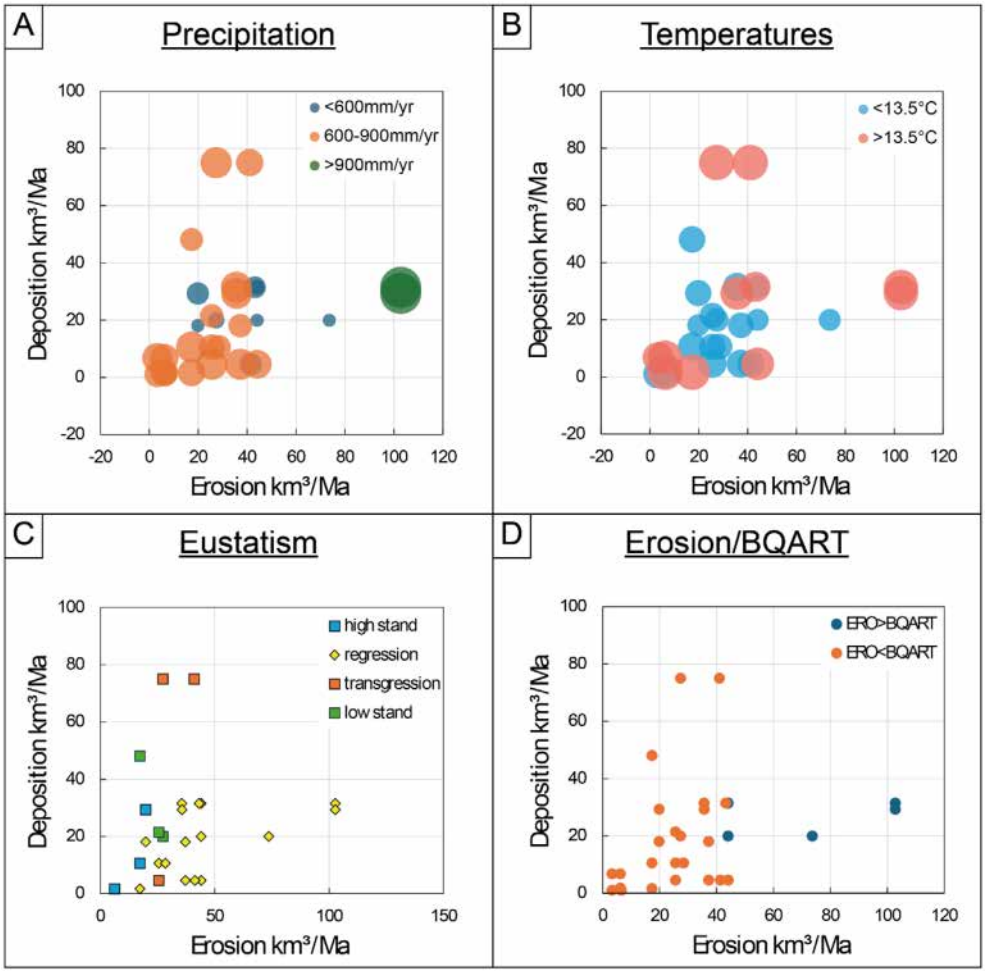

FIGURE 9 | Deposited fluxes (preferred scenario) against erosional fluxes (scenario A) (km^3/Ma) as a function of (A) precipitation, (B) temperature (C) eustatic trends of 100kyr cycles and (D) the erosion-BQART ratio; the size of the points in graphs (A) and (B) represents the precipitation or temperature value estimated by the palynological study of Mommersteeg et al. (1995) (see Table S4 of Supporting Information for data).

Erosional fluxes appear to remain low during regression periods, as well as when the temperatures and precipitations remain low (glacial periods). Erosional fluxes, although low, are nevertheless higher than those estimated from the BQART model during the regression phase between 103 and 96 and between 76 and 37.5 ka (Figure 9D). Furthermore, deposition flux rates seem to increase during the low stands of glacial periods. The Holocene period (12–0 ka) is the only period with very high depositional fluxes combined with mean erosional fluxes and high suspended load fluxes (BQART), during a transgressive period with high temperatures and mean precipitations.

5 | Discussion

5.1 | Mass Balance Limits and Signal Trends Uncertainties

In this section, we discuss the limitations of our approaches both in terms of data processing and the geological model. Even though the three sedimentary signals are similar despite the erosional or depositional fluxes being low (Figure 8), we observe that the erosional fluxes are twice as high as the depositional fluxes. In this study, we have considered very extreme scenarios in an attempt to cover as far as possible the uncertainties in the methods for reconstructing eroded and deposited volumes. When we compare our minimum erosion results with the maximum deposition results for each time interval, we find that erosion is almost systematically greater than deposition. Therefore, we think that this observation may suggest a signal attenuation. It is possible that some of the eroded sediments did not reach the deposition zone. Some of the eroded sediments may have been deposited in the littoral zone, as indicated by the presence of several Gilbert-type deltas currently onshore. Indeed, the coastline was located further south during the 800–400 ka period than it is today, so if sediments eroded during this period were deposited close to the palaeo-coastline, they would be located in the currently emerged part of the basin and would not have been considered in the quantification of sediments deposited during this period.

The recording of the sedimentary signal may have been affected by phenomena such as time lags, buffering or signal shredding, which may be superimposed by a Sadler effect. The Sadler effect is linked to the fact of having an irregular sampling step, which can bring out very marked peaks over very short periods of time (Sadler 1999; Schumer and Jerolmack 2009). Here, the fluxes calculated for erosion and

deposition have long time intervals during the 800–400 ka period (step duration of 100 to 200 ka for erosion and 30 to 250 ka for deposition). We studied the relationship between time span and sediment fluxes and observed this effect for the fluxes in the three parts of the system. Consequently, we calculated erosion fluxes, suspended fluxes et depositional fluxes over three even time intervals (10, 20 and 50 ka) in the same way as Rouby et al. (2023) (see Figure S3 of Supporting Information). Even with a time interval of 50 ka, the gradual increase is preserved just like the peaks at 200 and 120 ka for erosion and deposition. This homogenous resampling suggests that the main trends of fluxes described above are preserved. The rapid variations recorded by the BQART method are strongly affected by this resampling and no major peak emerges. Despite the possibility of a Sadler effect for some of the peaks for the BQART method, resampling indicates that trends and comparison between the three methods is still valid.

5.2 | Suspended Load Estimations

The fluxes calculated from the catchment erosion, BQART method and basin sedimentation are of the same order of magnitude. However, BQART model fluxes are overall higher than erosion fluxes, which are themselves higher than deposition fluxes. Without considering second order variations within climatic cycles, this long-term increase corresponds to a factor of 2.2, 6 and 40, respectively, for the BQART model, erosion and deposition. The signal for erosion (from both catchment reconstruction and the BQART model) is much greater than that for deposition. Overall, the fluxes from the BQART model are much greater than those from erosion and deposition, especially for the 800–400 ka period. It is possible that fluxes are underestimated for erosion and probably more so for deposition due to a potential hiatus and signal attenuation (see part 5.1). It is also possible that the BQART may overestimate sediment fluxes as the BQART is an empirical model for suspended sediment loads whose predictions range on a factor of 2–5 and as one of its parameters is based on maximum relief over the entire period. However, the BQART model fluxes are so significantly higher than the two other methods, particularly for the 800–400 ka period, that we consider that this overestimation cannot be solely the result of the relief parameter or a signal shredding (see part 5.1).

The other parametric difference between the BQART model and the other methods concerns the climatic parameters (temperatures and precipitations): these parameters were not considered in our reconstructions of erosional and depositional sediment fluxes. It is very likely that these climatic parameters contribute to an overestimation of the fluxes from the BQART model compared with the fluxes from the other methods. As indicated above, not only does the BQART model give a higher flux estimate than the other two methods, but the fluxes recorded by erosion and sedimentation are very low, 1–7.0 km^3/Ma for the 800–700 kyr period (compared with 25.0 km^3/Ma for the BQART) for example. The BQART model is based on climatic factors taken from Mommersteeg et al. (1995), in addition to catchment area and relief. One possible explanation for the difference between the BQART method and the other two methods is that in BQART, climatic parameters take precedence over parameters related to the growing area and relief. The climatic data set comes from the Tenagi Philippon cores that are located around 300 km away in a more stable, probably colder, area, so an overestimation in our study area is unlikely. Furthermore, the surface area and relief of the catchment area could have been much smaller if, as previously discussed, we consider the scenario of capturing upstream areas with high relief; this would have led to an overestimation of the BQART model flux. Nevertheless, the BQART model is based on climate data whose resolution makes it possible to describe cyclicity in sediment fluxes, which are around 35% higher during interglacial periods than during glacial periods. The other methods we used do not allow these fluxes to be discussed as finely as those calculated by the BQART model.

5.3 | Large Scale Trends in the Sediment Budget

The comparison of results for erosional, BQART model and depositional fluxes shows that estimates derived from the sink environment (deposition) are generally lower than those from the source environment (erosion and BQART), which may correspond to an attenuation of the sedimentary signal in the system between source and sink. The comparison also indicates that the increase in sediment flux from 800 ka to present day is a robust signal. We suggest that the gradual growth shown in the three histograms (Figure 8) is primarily set by the increase in the size of the catchment produced by the regional uplift. The Sithas catchment is estimated to have increased threefold for both 'thin' and 'wide' palaeo-catchment reconstructions (see Figure S1 of Supporting Information). The growth of the catchment has a direct impact on the BQART model and erosion assessments as the catchment area is a key parameter in this regression model, where larger catchments are expected to export more sediments. It is also possible that the climatic signal grew in intensity from 400 ka onwards, such that it overcame the internal autogenic dynamics of the sedimentary system or the signal related to the catchment's growth, leading to a signal increase in the fluxes. Another possibility is that the growth of the catchment began to resonate with the frequency of climate cycles, such that the signal was amplified by the sediment transport (Godard et al. 2013). A last hypothesis could be that the Sithas system was in a transient stage of evolution during the last 800 kyr: numerical models show a gradual increase of erosional rates similar to our observations in the case of systems where the connectivity time is significant compared with the time required for the system to reach a steady state (Carretier et al. 2009).

Due to the higher age model resolution, a cyclicity with a period of 90 up to 170 kyr can be observed in the record since 370 ka. This cyclicity seems in phase with the glacial–interglacial cyclicity characterised by the Marine Isotope Stages (MIS): there is a peak of erosional fluxes during interglacial periods and lower fluxes during glacial periods and low depositional fluxes during interglacial periods and peaks of fluxes during glacial periods. Interglacial periods are characterised by a high eustatic sea level, stronger precipitation and elevated temperature in the Gulf of Corinth region, unlike the glacial periods, which were characterised by low to medium levels of precipitation (Mommersteeg et al. 1995; Tzedakis et al. 2006;

McNeill et al. 2019). Rising eustatic level will limit headward erosion within the catchment and therefore could reduce sediment fluxes (Castelltort et al. 2023). However, a warm and humid climate will lead to increased erosion within the catchment (Syvitski and Milliman 2007; Watkins et al. 2019). A combined source-to-sink model suggests that, while downstream, sea-level rise could cause transgression and landward migration of the shoreline location, precipitation change would impact the whole catchment, generating increased sediment fluxes and instead cause basinward migration of the shoreline through propagation via enhanced sediment flux (Armitage et al. 2018). Given that the observations are of increased erosional fluxes during high-stand periods, we would suggest that the ~100 kyr cyclicity is caused by increased precipitation and temperature during interglacial periods (Figure 9). However, this cyclicity could be an artefact of the time intervals within the record (see part 5.1). We sub-sampled the observed sediment fluxes to time intervals of 10, 20 and 50 ka (see Supporting Information) and it was found that the cyclical peaks and troughs in sediment flux were robust even when sub-sampled, suggesting that this is a signal of external forcing likely related to sea level and climatic variations. Moreover, regional climate was not fixed for the last 800 ka: intensity of the glacial–interglacial cycles with 100–120 kyr periods has increased since the Early-Middle Pleistocene (Masson-Delmotte et al. 2010; Head and Gibbard 2015). Head and Gibbard (2015) suggested that: (1) climatic cyclicity began at ~1.4 Ma, marked by a low-frequency variability (two to three bundled obliquity cycles) since 1.25–1.20 Ma, a strengthening at ~1000–900 ka to get the current intensity from ~700–650 ka; (2) the orbital parameter changes generate higher amplitude interglacial than before and high asymmetrical variability (strong linear forcing) of ~100 kyr climatic cycles and (3) interglacial temperatures abruptly increased soon after the Mid-Brunhes Event (MIS 12/11). These different hypotheses may contribute to the increase of sediment fluxes in the system, but it is difficult to conclude on the predominance of one of them.

Another reason for the change in sediment flux at 400 ka could be due to the change in the regional tectonics of the Gulf of Corinth from around 400 ka. Nixon et al. (2016) proposed a migration from a deformation focused on individual north and south dipping faults to a deformation localised on north dipping faults due to the decrease in activity of the major south dipping faults. It can be observed in the central rift where the north dipping faults accommodate most of the deformation since ~340 ka with slip rates up to 3.5–6 mm/yr for the Xylokastro fault (Nixon et al. 2024), associated with a single major depocenter along the southern margin of the Gulf of Corinth on the hanging wall and an increase of erosion in the footwall. These tectonic changes affected both the eastern and western boundaries of the Gulf of Corinth (Collier 1990; Gawthorpe et al. 2022).

5.4 | Comparison Between Erosion and Deposition: System Dynamics Linked to the Storage Capacity of the Transfer Zone

The last cycle's higher resolution (between 103 and 12 ka) means a better understanding of the change in sediment flux over time in the source and sink regions. In this section, we compare in more detail the different flux evolutions (erosion, deposition, BQART) and establish a model representing the evolution of the Sithas system for the 370–12 ka period (Figure 10). This system is characterised by two successive dynamics: one out of phase, the other corresponding to the transition between an out-of-phase system and an in-phase system.

The first dynamics of the coupled system, between 370 and 103 ka, show erosion and deposition being out of sync and occurring at different times during an eustatic cycle, which can be summed up in two phases: (1) A first phase of strong erosional flux happening during high sea level, with high precipitation and temperatures, during which sediments are massively transported towards the catchment outlet, but depositional sediment fluxes remain very low in comparison. As the catchment's outlet is distant from the submarine canyon, some sediment may be stored between the coast and the canyon. (2) A second phase during lowstands, when there is lower erosion in the catchment and peaks of deposition in the deep-sea fan. These peaks may be generated by the remobilisation of sediments deposited along the coast after the sea level drop and the shoreline migration. These sediments would then be exported to the most distal part of the system: the deep-sea fan. The temporary storage area would gradually get smaller over time (Figure 10A).

The second dynamic begins at 103 ka and consists of four phases corresponding to the transition from an out-of-phase system to an in-phase system. (1) The first phase (MIS 5e to MIS 5c) is characterised by strong erosional fluxes and moderate depositional fluxes during a warm and humid (> 800 mm/yr) high-stand, with sediments stored in a small temporary storage area between the catchment and the deep-sea fan. (2) In the second phase (MIS 5b to MIS 4), erosional fluxes are lower than during the previous period and the depositional fluxes are higher. This coincides with low to medium precipitation, cool temperatures and the reduction of the temporary storage area as the coastline migrates basinwards and the sediments in this area are exported to the sink. (3) The third stage coincides with the regression from MIS 5c to MIS 3a, a period of low to medium precipitations and low temperatures. As the coastline is moving basinwards, the temporary storage area got smaller and smaller. Erosional fluxes are very high, but depositional fluxes are much lower than before. (4) The last stage corresponds to the last glacial lowstand. Erosional and depositional fluxes are the lowest, as are temperatures and precipitation and synchronous. The storage area is small or non-existent and the catchment is directly connected to the deep-sea fan via a submarine canyon (Figure 10B).

Finally, the Holocene period is characterised by first medium to high fluxes in the source and the sink during the transgression as the start of a new dynamic. The sink and source zones of our system are synchronised, which seems to be linked to the disappearance of the temporary storage area between the shoreline and the submarine canyon, allowing sediment to be transported directly to the deep-sea fan. The size of this temporary storage area is linked to coastal migration, which is controlled by eustatic variations and uplift.

Previous studies in the Corinth Gulf at different scales (Alkyonides basin, eastern part of the Gulf of Corinth) have

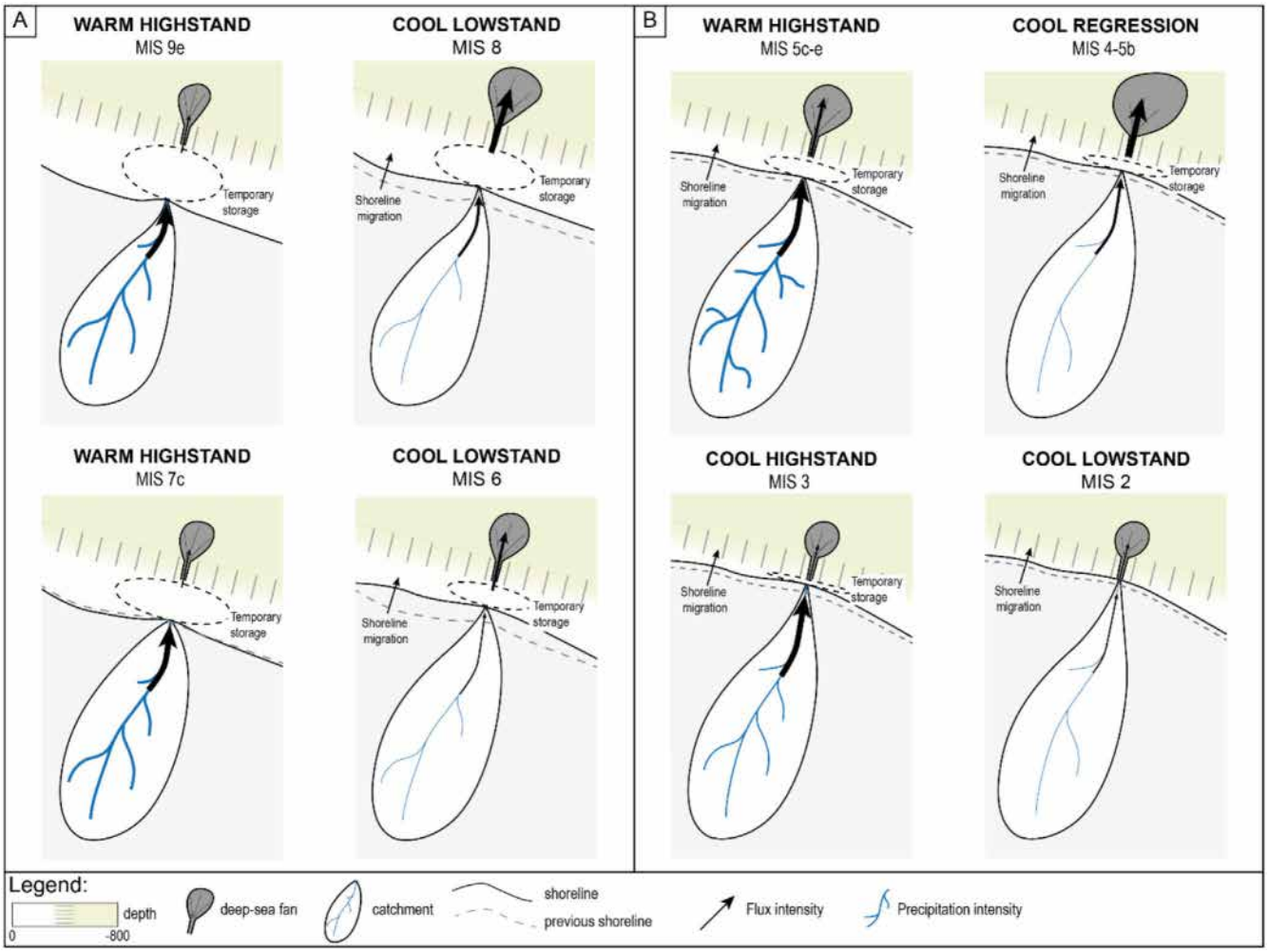

FIGURE 10 | Schematic of the evolution of the Sithas system in the last 370 kyr, line thickness for precipitations and fluxes corresponds to the intensity of these phenomena. (A) Dynamic of the system between 370 and 130 ka. (B) Dynamic of the system between 130 and 12 ka.

mainly focused on the last 250 or 130 kyr in the basin part and found that the amount of sediment deposited is higher during glacial periods, when there is less vegetation and less rain (Collier et al. 2000; McNeill et al. 2019; Mohamed et al. 2024). We made the same observations on the sink part of the Sithas system without linking it to the change in vegetation. However, Watkins et al. (2019) show that, in the Gulf of Corinth, there is more sediment deposited during the last interglacial period (Holocene) and they hypothesise that erosion is also greater during these periods. This matches our estimates of eroded sediment fluxes, both in glacial and interglacial periods but not with our estimations of deposited fluxes. These opposite results lead to our hypothesis of a desynchronisation of the system induced by a temporary storage zone between the source and the sink areas. Phase shifting of fluxes seems to be possible only in very specific cases, such as the Sithas system, due to the disconnection of the catchment from its deep-sea fan.

6 | Conclusion

We quantified, for the first time, the fluxes of sediment in erosion and deposition across the entire S2S system of Sithas (Greece) for the last 800 kyr by: (1) restoring the volume of sediment eroded in the catchment, (2) upgrading the age model and quantifying the volume of sediment deposited and (3) quantifying erosion fluxes by the BQART method.

Each of the three methods shows a gradual increase of the fluxes since 800 ka and more specifically since 400 ka. This gradual increase reflects the expansion of the catchment area in response to tectonic uplift. From this time, we record two different types of sedimentary cycles influenced by the climatic signal. The first one is out of phase between the source and the sink, while the second one is gradually becoming in sync. The lack of recorded cycles between 800 and 400 ka could be explained by a transient state of the system. The period from 400 kyr coincides with a change in climate, with an intensification of glacial cycles and in tectonic terms, with a migration of the deformation from the west of the Gulf of Corinth towards the centre and the Xylokastro region.

The erosion and deposition fluxes are not in phase during the 310–103 ka period. Both erosion and deposition show a cyclicity of climatic origin, but the flux peaks are occurring during interglacial periods for the erosion and glacial periods for the deposition. We hypothesise that this desynchronisation is the result of temporary storage of sediment in the

system, probably at the land-sea interface and we developed a synthetic model. Climatic conditions favourable to erosion during interglacial periods produce a peak flux in the source part and the sediments are stored in the temporary storage area. The flux decreases during the glacial period, as eroded sediments cannot be transported due to low export capacities. The stored sediments are then remobilised during the glacial periods and exported to the deep-sea fan, leading to a peak in deposition flux. During the 103–12 ka period, erosion and deposition fluxes were reorganised to follow an in-phase dynamic, suggesting a full connection between the river and the submarine canyon.

The Sithas system shows the evolution of a complete S2S system during several eustatic and climatic cycles constrained by regional uplift. It would be of interest to study other coupled S2S systems to determine whether this model can be generalised and especially whether and how the size of the system impact the resulting concepts. It would also be of interest to study the Sithas system at a higher temporal resolution. This could improve the understanding of the transition periods between the phases of preservation of the marine terraces, especially for the last glacial–interglacial quaternary cycle.

Acknowledgements

This research was funded by the Institute IFPEN. We would like to thank D. Sakellariou for the availability of the seismic data, M. Loubrie and J.C. Lecomte for the seismic data analysis and support to quantify sediment deposited volumes. We also would like to thank D. Rouby for her feedback about the impact of the Sadler effect. We are grateful to Leonardo Muniz-Pichel (Associate Editor) and Robert Duller, Alex Whittaker and Tim Cullen (Reviewers), whose detailed comments helped us to substantially improve our manuscript.

Conflicts of Interest

The authors declare no conflicts of interest.

Data Availability Statement

The data that supports the findings of this study are available in the Supporting Information of this article.

Peer Review

The peer review history for this article is available at https://www.webofscience.com/api/gateway/wos/peer-review/10.1111/bre.70044.

References

Allen, P. A. 2008. "Time Scales of Tectonic Landscapes and Their Sediment Routing Systems." *Geological Society, London, Special Publications* 296: 7–28. https://doi.org/10.1144/SP296.2.

Armijo, R., B. Meyer, G. King, A. Rigo, and D. Papanastassiou. 1996. "Quaternary Evolution of the Corinth Rift and Its Implications for the Late Cenozoic Evolution of the Aegean." *Geophysical Journal International* 126, no. 1: 11. https://doi.org/10.1111/j.1365-246X.1996.tb05264.x.

Armitage, J. J., P. M. Burgess, G. J. Hampson, and P. A. Allen. 2018. "Deciphering the Origin of Cyclical Gravel Front and Shoreline Progradation and Retrogradation in the Stratigraphic Record." *Basin Research* 30, no. S1: 15–35. https://doi.org/10.1111/bre.12203.

Armitage, J. J., R. A. Duller, A. C. Whittaker, and P. A. Allen. 2011. "Transformation of Tectonic and Climatic Signals From Source to Sedimentary Archive." *Nature Geoscience* 4, no. 4: 231–235. https://doi.org/10.1038/ngeo1087.

Baudin, F., C. Rabouille, and B. Dennielou. 2020. "Routing of Terrestrial Organic Matter From The Congo River to the Ultimate Sink in the Abyss: A Mass Balance Approach (André Dumont Medallist Lecture 2017)." *Geologica Belgica* 23, no. 1–2: xx. https://doi.org/10.20341/gb.2020.004.

Braun, J., C. Voisin, A. T. Gourlan, and C. Chauvel. 2015. "Erosional Response of an Actively Uplifting Mountain Belt to Cyclic Rainfall Variations." *Earth Surface Dynamics* 3, no. 1: 1–14. https://doi.org/10.5194/esurf-3-1-2015.

Briole, P., A. Rigo, H. Lyon-Caen, et al. 2000. "Active Deformation of the Corinth Rift, Greece: Results From Repeated Global Positioning System Surveys Between 1990 and 1995." *Journal of Geophysical Research: Solid Earth* 105, no. B11: 25605–25625. https://doi.org/10.1029/2000JB900148.

Carretier, S., B. Poisson, R. Vassallo, E. Pepin, and M. Farias. 2009. "Tectonic Interpretation of Transient Stage Erosion Rates at Different Spatial Scales in an Uplifting Block." *Journal of Geophysical Research: Earth Surface* 114, no. F2. https://doi.org/10.1029/2008JF001080.

Carretier, S., V. Regard, L. Leanni, and M. Farías. 2019. "Long-Term Dispersion of River Gravel in a Canyon in the Atacama Desert, Central Andes, Deduced From Their 10Be Concentrations." *Scientific Reports* 9, no. 1: 17763. https://doi.org/10.1038/s41598-019-53806-x.

Castelltort, S., C. Fillon, É. Lasseur, et al. 2023. *The Source-To-Sink Vade-Mecum: History, Concepts and Tools|Vade-Mecum de L'approche Source-To-Sink: Histoire, Concepts et Outils*. SEPM (Society for Sedimentary Geology).

Castelltort, S., and J. van den Driessche. 2003. "How Plausible Are High-Frequency Sediment Supply-Driven Cycles in the Stratigraphic Record?" *Sedimentary Geology* 157, no. 1-2: 3–13. https://doi.org/10.1016/S0037-0738(03)00066-6.

Collier, R. E. 1990. "Eustatic and Tectonic Controls Upon Quaternary Coastal Sedimentation in the Corinth Basin, Greece." *Journal of the Geological Society* 147, no. 2: 301–314. https://doi.org/10.1144/gsjgs.147.2.0301.

Collier, R. E., M. R. Leeder, M. Trout, G. Ferentinos, E. Lyberis, and G. Papatheodorou. 2000. "High Sediment Yields and Cool, Wet Winters: Test of Last Glacial Paleoclimates in the Northern Mediterranean." *Geology* 28, no. 11: 999. https://doi.org/10.1130/0091-7613(2000)28<999:HSYACW>2.0.CO;2.

Collier, R. E. L., M. R. Leeder, P. J. Rowe, and T. C. Atkinson. 1992. "Rates of Tectonic Uplift in the Corinth and Megara Basins, Central Greece." *Tectonics* 11, no. 6: 1159–1167. https://doi.org/10.1029/92TC01565.

de Gelder, G., D. Fernández-Blanco, D. Melnick, et al. 2019. "Lithospheric Flexure and Rheology Determined by Climate Cycle Markers in the Corinth Rift." *Scientific Reports* 9, no. 1: 4260. https://doi.org/10.1038/s41598-018-36377-1.

de Gelder, G., J. Jara-Muñoz, D. Melnick, et al. 2020. "How Do Sea-Level Curves Influence Modeled Marine Terrace Sequences?" *Quaternary Science Reviews* 229: 106132. https://doi.org/10.1016/j.quascirev.2019.106132.

de Lavaissière, L., S. Bonnet, A. Guyez, and P. Davy. 2022. "Autogenic Knickpoints in Laboratory Landscape Experiments." *Earth Surface Dynamics* 10, no. 2: 229–246. https://doi.org/10.5194/esurf-10-229-2022.

Demoulin, A., A. Beckers, and A. Hubert-Ferrari. 2015. "Patterns of Quaternary Uplift of the Corinth Rift Southern Border (N Peloponnese, Greece) Revealed by Fluvial Landscape Morphometry." *Geomorphology* 246: 188–204. https://doi.org/10.1016/j.geomorph.2015.05.032.

Dia, A., A. Cohen, R. O'Nions, and J. Jackson. 1997. "Rates of Uplift Investigated Through 230Th Dating in the Gulf of Corinth (Greece)." *Chemical Geology* 138, no. 3-4: 171–184. https://doi.org/10.1016/S0009-2541(97)00010-7.

Duller, R. A., J. J. Armitage, H. R. Manners, S. Grimes, and T. D. Jones. 2019. "Delayed Sedimentary Response to Abrupt Climate Change at the Paleocene-Eocene Boundary, Northern Spain." *Geology* 47, no. 2: 159–162. https://doi.org/10.1130/G45631.1.

Gawthorpe, R. L., N. Fabregas, S. Pechlivanidou, et al. 2022. "Late Quaternary Mud-Dominated, Basin-Floor Sedimentation of the Gulf of Corinth, Greece: Implications for Deep-Water Depositional Processes and Controls on Syn-Rift Sedimentation." *Basin Research* 34, no. 5: 1567–1600. https://doi.org/10.1111/bre.12671.

Godard, V., G. E. Tucker, G. Burch Fisher, D. W. Burbank, and B. Bookhagen. 2013. "Frequency-Dependent Landscape Response to Climatic Forcing." *Geophysical Research Letters* 40, no. 5: 859–863. https://doi.org/10.1002/grl.50253.

Griffin, C., R. A. Duller, and K. M. Straub. 2023. "The Degradation and Detection of Environmental Signals in Sediment Transport Systems." *Science Advances* 9, no. 44: eadi8046. https://doi.org/10.1126/sciadv.adi8046.

Guillocheau, F., D. Rouby, C. Robin, et al. 2012. "Quantification and Causes of the Terrigeneous Sediment Budget at the Scale of a Continental Margin: A New Method Applied to the Namibia–South Africa Margin." *Basin Research* 24, no. 1: 3–30. https://doi.org/10.1111/j.1365-2117.2011.00511.x.

Guyez, A., S. Bonnet, T. Reimann, S. Carretier, and J. Wallinga. 2023. "A Novel Approach to Quantify Sediment Transfer and Storage in Rivers—Testing Feldspar Single-Grain pIRIR Analysis and Numerical Simulations." *Journal of Geophysical Research: Earth Surface* 128, no. 2: e2022JF006727. https://doi.org/10.1029/2022JF006727.

Head, M. J., and P. L. Gibbard. 2015. "Early–Middle Pleistocene Transitions: Linking Terrestrial and Marine Realms." *Quaternary International* 389: 7–46. https://doi.org/10.1016/j.quaint.2015.09.042.

Hinderer, M. 2012. "From Gullies to Mountain Belts: A Review of Sediment Budgets at Various Scales." *Sedimentary Geology* 280: 21–59. https://doi.org/10.1016/j.sedgeo.2012.03.009.

Jerolmack, D. J., and C. Paola. 2010. "Shredding of Environmental Signals by Sediment Transport." *Geophysical Research Letters* 37, no. 19. https://doi.org/10.1029/2010GL044638.

Jones, M. A., P. L. Heller, E. Roca, M. Garcés, and L. Cabrera. 2004. "Time Lag of Syntectonic Sedimentation Across an Alluvial Basin: Theory and Example From the Ebro Basin, Spain." *Basin Research* 16, no. 4: 489–506. https://doi.org/10.1111/j.1365-2117.2004.00244.x.

Keraudren, B., and D. Sorel. 1987. "The Terraces of Corinth (Greece)—A Detailed Record of Eustatic Sea-Level Variations During the Last 500,000 Years." *Marine Geology* 77, no. 1-2: 99–107. https://doi.org/10.1016/0025-3227(87)90085-5.

Leeder, M. R., C. Portman, J. E. Andrews, et al. 2005. "Normal Faulting and Crustal Deformation, Alkyonides Gulf and Perachora Peninsula, Eastern Gulf of Corinth Rift, Greece." *Journal of the Geological Society* 162, no. 3: 549–561. https://doi.org/10.1144/0016-764904-075.

Lykousis, V., D. Sakellariou, I. Moretti, and H. Kaberi. 2007. "Late Quaternary Basin Evolution of the Gulf of Corinth: Sequence Stratigraphy, Sedimentation, Fault–Slip and Subsidence Rates." *Tectonophysics* 440, no. 1-4: 29–51. https://doi.org/10.1016/j.tecto.2006.11.007.

Masson-Delmotte, V., B. Stenni, K. Pol, et al. 2010. "EPICA Dome C Record of Glacial and Interglacial Intensities." *Quaternary Science Reviews* 29, no. 1-2: 113–128. https://doi.org/10.1016/j.quascirev.2009.09.030.

McNab, F., T. F. Schildgen, J. M. Turowski, and A. D. Wickert. 2023. "Diverse Responses of Alluvial Rivers to Periodic Environmental Change." *Geophysical Research Letters* 50, no. 10: e2023GL103075. https://doi.org/10.1029/2023GL103075.

McNeill, L. C., D. J. Shillington, G. D. O. Carter, et al. 2019. "High-Resolution Record Reveals Climate-Driven Environmental and Sedimentary Changes in an Active Rift." *Scientific Reports* 9, no. 1: 3116. https://doi.org/10.1038/s41598-019-40022-w.

Mohamed, M. A., R. E. L. Collier, D. M. Hodgson, et al. 2024. "Sediment Flux Variation as a Record of Climate Change in the Late Quaternary Deep-Water Active Corinth Rift, Greece." *Basin Research* 36, no. 5: e12896. https://doi.org/10.1111/bre.12896.

Mommersteeg, H. J. P. M., M. F. Loutre, R. Young, T. A. Wijmstra, and H. Hooghiemstra. 1995. "Orbital Forced Frequencies in the 975 000 Year Pollen Record From Tenagi Philippon (Greece)." *Climate Dynamics* 11, no. 1: 4–24. https://doi.org/10.1007/BF00220674.

Moretti, I., V. Lykousis, D. Sakellariou, J.-Y. Reynaud, B. Benziane, and A. Prinzhoffer. 2004. "Sedimentation and Subsidence Rate in the Gulf of Corinth: What We Learn From the Marion Dufresne's Long-Piston Coring." *Comptes Rendus Geoscience* 336, no. 4-5: 291–299. https://doi.org/10.1016/j.crte.2003.11.011.

Moretti, I., D. Sakellariou, V. Lykousis, and L. Micarelli. 2003. "The Gulf of Corinth: An Active Half Graben?" *Journal of Geodynamics* 36, no. 1–2: 323–340. https://doi.org/10.1016/S0264-3707(03)00053-X.

Moussirou, B., and S. Bonnet. 2018. "Modulation of the Erosion Rate of an Uplifting Landscape by Long-Term Climate Change: An Experimental Investigation." *Geomorphology* 303: 456–466. https://doi.org/10.1016/j.geomorph.2017.12.010.

Muravchik, M., G. A. Henstra, G. T. Eliassen, et al. 2020. "Deep-Water Sediment Transport Patterns and Basin Floor Topography in Early Rift Basins: Plio-Pleistocene Syn-Rift of the Corinth Rift, Greece." *Basin Research* 32, no. 5: 1184–1212. https://doi.org/10.1111/bre.12423.

Nixon, C. W., L. C. McNeill, J. M. Bull, et al. 2016. "Rapid Spatiotemporal Variations in Rift Structure During Development of the Corinth Rift, Central Greece." *Tectonics* 35, no. 5: 1225–1248. https://doi.org/10.1002/2015TC004026.

Nixon, C. W., L. C. McNeill, R. L. Gawthorpe, et al. 2024. "Increasing Fault Slip Rates Within the Corinth Rift, Greece: A Rapidly Localising Active Rift Fault Network." *Earth and Planetary Science Letters* 636: 118716. https://doi.org/10.1016/j.epsl.2024.118716.

Nyberg, B., W. Helland-Hansen, R. Gawthorpe, F. Tillmans, and P. Sandbakken. 2021. "Assessing First-Order BQART Estimates for Ancient Source-To-Sink Mass Budget Calculations." *Basin Research* 33, no. 4: 2435–2452. https://doi.org/10.1111/bre.12563.

Ori, G. G. 1989. "Geologic History of the Extensional Basin of the Gulf of Corinth (?Miocene-Pleistocene), Greece." *Geology* 17, no. 10: 918. https://doi.org/10.1130/0091-7613(1989)017<0918:GHOTEB>2.3.CO;2.

Pazzaglia, F. J., and M. T. Brandon. 1996. "Macrogeomorphic Evolution of the Post-Triassic Appalachian Mountains Determined by Deconvolution of the Offshore Basin Sedimentary Record." *Basin Research* 8, no. 3: 255–278. https://doi.org/10.1046/j.1365-2117.1996.00274.x.

Pedoja, K., L. Husson, M. E. Johnson, et al. 2014. "Coastal Staircase Sequences Reflecting Sea-Level Oscillations and Tectonic Uplift During the Quaternary and Neogene." *Earth-Science Reviews* 132: 13–38. https://doi.org/10.1016/j.earscirev.2014.01.007.

Railsback, L. B., P. L. Gibbard, M. J. Head, N. R. G. Voarintsoa, and S. Toucanne. 2015. "An Optimized Scheme of Lettered Marine Isotope Substages for the Last 1.0 Million Years, and the Climatostratigraphic Nature of Isotope Stages and Substages." *Quaternary Science Reviews* 111: 94–106. https://doi.org/10.1016/j.quascirev.2015.01.012.

Repasch, M., H. Wittmann, J. S. Scheingross, et al. 2020. "Sediment Transit Time and Floodplain Storage Dynamics in Alluvial Rivers Revealed by Meteoric 10 be." *Journal of Geophysical Research: Earth*

Surface 125, no. 7: e2019JF005419. https://doi.org/10.1029/2019JF005419.

Rohais, S., S. Bonnet, and R. Eschard. 2012. "Sedimentary Record of Tectonic and Climatic Erosional Perturbations in an Experimental Coupled Catchment-Fan System." *Basin Research* 24, no. 2: 198–212. https://doi.org/10.1111/j.1365-2117.2011.00520.x.

Rohais, S., R. Eschard, M. Ford, F. Guillocheau, and I. Moretti. 2007. "Stratigraphic Architecture of the Plio-Pleistocene Infill of the Corinth Rift: Implications for Its Structural Evolution." *Tectonophysics* 440, no. 1-4: 5–28. https://doi.org/10.1016/j.tecto.2006.11.006.

Rohais, S., J. P. Lovecchio, V. Abreu, M. Miguez, and S. Paulin. 2021. "High-Resolution Sedimentary Budget Quantification—Example From the Cenozoic Deposits in the Pelotas Basin, South Atlantic." *Basin Research* 33, no. 4: 2252–2280. https://doi.org/10.1111/bre.12556.

Rohais, S., and I. Moretti. 2017. *Structural and Stratigraphic Architecture of the Corinth Rift (Greece): An Integrated Onshore to Offshore Basin-Scale Synthesis: Lithosphere Dynamics and Sedimentary Basins of the Arabian Plate and Surrounding Areas*, 89–120. https://doi.org/10.1007/978-3-319-44726-1_5.

Romans, B. W., S. Castelltort, J. A. Covault, A. Fildani, and J. P. Walsh. 2016. "Environmental Signal Propagation in Sedimentary Systems Across Timescales." *Earth-Science Reviews* 153: 7–29. https://doi.org/10.1016/j.earscirev.2015.07.012.

Ronov, A. B., V. E. Khain, A. N. Balukhovsky, and K. B. Seslavinsky. 1980. "Quantitative Analysis of Phanerozoic Sedimentation." *Sedimentary Geology* 25, no. 4: 311–325. https://doi.org/10.1016/0037-0738(80)90067-6.

Rouby, D., S. Bonnet, F. Guillocheau, et al. 2009. "Sediment Supply to the Orange Sedimentary System Over the Last 150My: An Evaluation From Sedimentation/Denudation Balance." *Marine and Petroleum Geology* 26, no. 6: 782–794. https://doi.org/10.1016/j.marpetgeo.2008.08.004.

Rouby, D., J. Ye, D. Chardon, A. Loparev, M. Wildman, and M. Dall'Asta. 2023. "Source-To-Sink Sedimentary Budget of the African Equatorial Atlantic Rifted Margin." *Geochemistry, Geophysics, Geosystems* 24, no. 12: e2023GC010901. https://doi.org/10.1029/2023GC010901.

Sadler, P. M. 1999. "The Influence of Hiatuses on Sediment Accumulation Rates." *GeoResearch Forum* 5: 15–40.

Sakellariou, D., V. Lykousis, S. Alexandri, et al. 2007. "Faulting, Seismic-Stratigraphic Architecture and Late Quaternary Evolution of the Gulf of Alkyonides Basin–East Gulf of Corinth, Central Greece." *Basin Research* 19, no. 2: 273–295. https://doi.org/10.1111/j.1365-2117.2007.00322.x.

Schumer, R., and D. J. Jerolmack. 2009. "Real and Apparent Changes in Sediment Deposition Rates Through Time." *Journal of Geophysical Research: Earth Surface* 114, no. F3. https://doi.org/10.1029/2009JF001266.

Schumm, S. A., and D. K. Rea. 1995. "Sediment Yield From Disturbed Earth Systems." *Geology* 23, no. 5: 391. https://doi.org/10.1130/0091-7613(1995)023<0391:SYFDES>2.3.CO;2.

Sébrier, M. 1977. Tectonique recente d'une transversale a l'Arc Egeen: le Golfe de Corinthe et ses regions peripheriques Thèse de doctorat, Paris XI Orsay.

Shillington, D. J., L. C. McNeill, and G. D. O. Carter. 2019. "Expedition 381 Preliminary Report: Corinth Active Rift Development." International Ocean Discovery Program. https://doi.org/10.14379/iodp.pr.381.2019.

Simpson, G., and S. Castelltort. 2012. "Model Shows That Rivers Transmit High-Frequency Climate Cycles to the Sedimentary Record." *Geology* 40, no. 12: 1131–1134. https://doi.org/10.1130/G33451.1.

Somme, T. O., D. J. W. Piper, M. E. Deptuck, and W. Helland-Hansen. 2011. "Linking Onshore-Offshore Sediment Dispersal in the Golo Source-to-Sink System (Corsica, France) During the Late Quaternary." *Journal of Sedimentary Research* 81, no. 2: 118–137. https://doi.org/10.2110/jsr.2011.11.

Spratt, R. M., and L. E. Lisiecki. 2016. "A Late Pleistocene Sea Level Stack." *Climate of the Past* 12, no. 4: 1079–1092. https://doi.org/10.5194/cp-12-1079-2016.

Straub, K. M., R. A. Duller, B. Z. Foreman, and E. A. Hajek. 2020. "Buffered, Incomplete, and Shredded: The Challenges of Reading an Imperfect Stratigraphic Record." *Journal of Geophysical Research: Earth Surface* 125, no. 3: e2019JF005079. https://doi.org/10.1029/2019JF005079.

Syvitski, J. P. M., and J. D. Milliman. 2007. "Geology, Geography, and Humans Battle for Dominance Over the Delivery of Fluvial Sediment to the Coastal Ocean." *Journal of Geology* 115, no. 1: 1–19. https://doi.org/10.1086/509246.

Taylor, B., J. R. Weiss, A. M. Goodliffe, M. Sachpazi, M. Laigle, and A. Hirn. 2011. "The Structures, Stratigraphy and Evolution of the Gulf of Corinth Rift, Greece." *Geophysical Journal International* 185, no. 3: 1189–1219. https://doi.org/10.1111/j.1365-246X.2011.05014.x.

Toby, S. C., R. A. Duller, S. de Angelis, and K. M. Straub. 2019. "A Stratigraphic Framework for the Preservation and Shredding of Environmental Signals." *Geophysical Research Letters* 46, no. 11: 5837–5845. https://doi.org/10.1029/2019GL082555.

Tofelde, S., A. Bernhardt, L. Guerit, and B. W. Romans. 2021. "Times Associated With Source-to-Sink Propagation of Environmental Signals During Landscape Transience." *Frontiers in Earth Science* 9: 628315. https://doi.org/10.3389/feart.2021.628315.

Tzedakis, P. C., H. Hooghiemstra, and H. Pälike. 2006. "The Last 1.35 Million Years at Tenaghi Philippon: Revised Chronostratigraphy and Long-Term Vegetation Trends." *Quaternary Science Reviews* 25, no. 23–24: 3416–3430. https://doi.org/10.1016/j.quascirev.2006.09.002.

Watkins, S. E., A. C. Whittaker, R. E. Bell, et al. 2019. "Are Landscapes Buffered to High-Frequency Climate Change? A Comparison of Sediment Fluxes and Depositional Volumes in the Corinth Rift, Central Greece, Over the Past 130 k.y." *GSA Bulletin* 131, no. 3-4: 372–388. https://doi.org/10.1130/B31953.1.

Whipple, K. X. 2001. "Fluvial Landscape Response Time: How Plausible Is Steady-State Denudation?" *American Journal of Science* 301, no. 4-5: 313–325. https://doi.org/10.2475/ajs.301.4-5.313.

Whipple, K. X., and G. E. Tucker. 2002. "Implications of Sediment-Flux-Dependent River Incision Models for Landscape Evolution." *Journal of Geophysical Research: Solid Earth* 107, no. B2: ETG-3–1–ETG-3–20. https://doi.org/10.1029/2000JB000044.

Zelilidis, A. 2000. "Drainage Evolution in a Rifted Basin, Corinth Graben, Greece." *Geomorphology* 35, no. 1–2: 69–85. https://doi.org/10.1016/S0169-555X(00)00023-4.

Zhou, Z., A. C. Whittaker, R. E. Bell, and G. J. Hampson. 2024. "Unravelling Tectonic and Lithological Effects on Transient Landscapes in the Gulf of Corinth, Greece." *Basin Research* 36, no. 5: e12901. https://doi.org/10.1111/bre.12901.

Supporting Information

Additional supporting information can be found online in the Supporting Information section.